Controlling Electron Transfer in Polymer Matrices through Supramolecular Interactions

A Doctoral Thesis

by

Yilin Cao

Submitted to the Graduate School of Science, Osaka University

February, 2024

Acknowledgements

This research was carried out from 2018 to 2024 under the direction of Prof. Dr. Hiroyasu Yamaguchi at the Department of Macromolecular Science, Graduate School of Science, Osaka University. The author expresses deep gratitude to Professor Dr. Hiroyasu Yamaguchi for his continuing guidance and encouragement throughout the study. Grateful acknowledgements are made to Asst. Prof. Dr. Yuichiro Kobayashi for his continuing help, warm encouragement and kind advice.

The author express gratitude to Prof. Dr. Takahiro Sato, Prof. Dr. Ken Terao (Department of Macromolecular Science, Graduate School of Science, Osaka University), Prof. Dr. Yasuhisa Mizutani (Department of Chemistry, Graduate School of Science, Osaka University), Assoc. Prof. Dr. Syoji Ito and Asst. Prof. Dr. Hikaru Sotome (Division of Frontier Materials Science, Graduate School of Engineering Science, Osaka University) for their cooperation in the optical measurements. Special thanks to Prof. Dr. Yoshinori Takashima, Asst. Prof. Ryouhei Ikura and Dr. Changming Jin (Department of Macromolecular Science, Graduate School of Science, Osaka University) for their help in GPC measurements.

This thesis was reviewed by Prof. Dr. Hiroyasu Yamaguchi, Prof. Dr. Akihito Hashidzume and Prof. Dr. Ken Terao. The author appreciates their careful review and helpful comments on this thesis.

The author would like to express sincere gratitude to all members of the Yamaguchi laboratory for their cooperation and friendship. Heartfelt appreciation is extended to all friends, especially Ms. Xueting Sun, Mr. Naite Zhang, Mr. Pengyu Song, Mr. Xiaolong Liu, Dr. Yi Yang, and Dr. Weinan Cao, for their invaluable friendship. Special acknowledgements are made to Ms. Difei Wang and Dr. Jin Qian for their gentleness and companionship. Most importantly, the author wishes to express endless gratitude to his partner, Dr. Shiyu Yang; his grandfather, Mr. Weifu Cao; grandmother, Mrs. Yinsheng Wang; father, Mr. Lu Cao; mothers, Mrs. Chunlan Kang and Mrs. Jinxia Chen; aunt, Mrs. Wei Cao; uncle, Mr. Lixin Niu; and brothers, Mr. Haonan Cao and Mr. Yuhan Niu, for their unwavering care, support, encouragement, and kindness. Lastly, the author holds an endless love and memory for his late grandfather.

February, 2024

曹 艺霖

Yilin Cao

Contents

Chapter 1

General Introduction

1-1. Global energy crisis and the pursuit of sustainable energy

The 21st century is marked by a global energy crisis, fueled by soaring demand and dwindling fossil fuel reserves.[1–3] This crisis is further exacerbated by environmental concerns such as greenhouse gas emissions, which contribute to global warming and adversely affect biodiversity, water resources and ecosystem health.[4,5] In response, solar energy emerges as a promising solution, offering a sustainable alternative to fossil fuels. Its potential to significantly exceed current global energy needs positions it as a key player in future energy strategies.[6–8]

The transition from fossil fuels to renewable sources like solar, wind, hydro, and biomass is pivotal for sustainable development.[9–13] This shift, while essential for addressing energy scarcity, also aims to mitigate environmental impacts. Integrating renewable energy sources, however, involves overcoming technological, economic, and political challenges. Yet, the progress in renewable energy technologies, coupled with a growing global environmental consciousness, is gradually easing this transition.

Scientific research and innovation play a critical role in this shift, particularly in areas like artificial photosynthesis systems. The goal of artificial photosynthesis research is to emulate the natural conversion of solar energy into chemical energy, thereby contributing to the development of advanced systems for solar energy utilization.

1-2. Natural photosynthesis and photoinduced electron transfer

Natural photosynthesis exemplifies the most efficient energy conversion process known to sustain life on Earth.[14–16] This biological phenomenon, where solar energy is transformed into chemical energy, is fundamental to the survival of plants and all life forms. At the heart of this process are chlorophyll molecules, predominantly found in plant leaves and algae, that capture sunlight and act as natural solar energy converters.[17,18] Including chlorophyll, structurally analogous compounds like porphyrins, phthalocyanines (Fig. 1-1) and their derivatives, possessing extensive π-conjugated structure, are usually employed as antenna molecules in artificial photosynthesis systems or related research.[19–24]

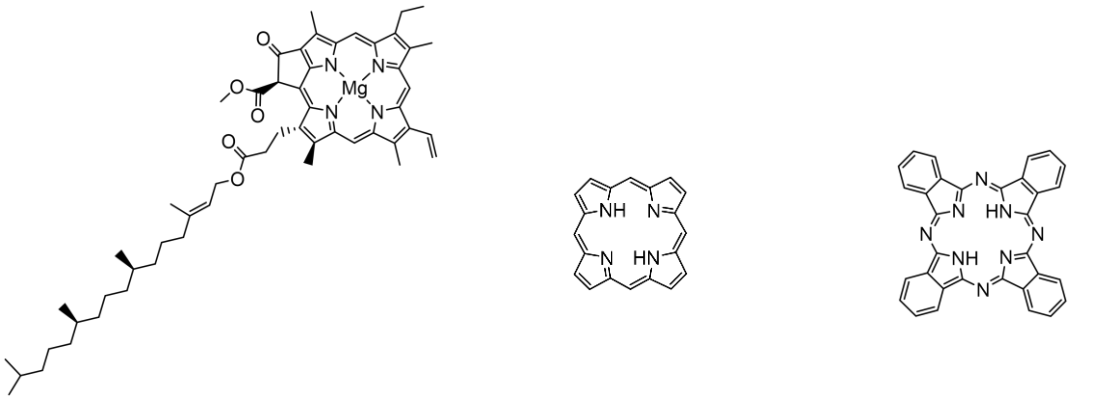

Fig. 1-1. Chemical structures of a) chlorophyll a, b) porphyrin and c) phthalocyanine.

Natural photosynthesis encompasses multiple stages, such as the light-dependent reactions[25,26] and the Calvin cycle.[27,28] In these stages, absorbed sunlight is used to produce energy-rich molecules like ATP and NADPH, which are then used to convert

atmospheric carbon dioxide into glucose.

Central to natural photosynthesis is the phenomenon of photoinduced electron transfer. This process begins when chlorophyll molecules absorb photons and reach an excited state, initiating electron transfer.[29,30] The electron transfer process in natural photosynthesis is usually not a singular event but a series of meticulously coordinated steps involving various electron donors and acceptors.[31–33] This intricate mechanism ensures efficient utilization and conversion of absorbed energy into a usable form. Each photosynthesis reaction center demonstrates precise structural organization, facilitating the efficient occurrence of photoinduced electron transfer processes.[34,35]

The reaction center in purple photosynthetic bacterium showcases a sophisticated structural organization vital for efficient electron transfer (Fig. 1-2). This intricate assembly, encompassing chlorophylls, quinones, and surrounding protein matrices, orchestrates a finely tuned electron transport chain. Spatial arrangement of protein matrices optimizes the distance between electron donors and acceptors, ensuring rapid and efficient electron transfer while minimizing energy dissipation. [36–38]

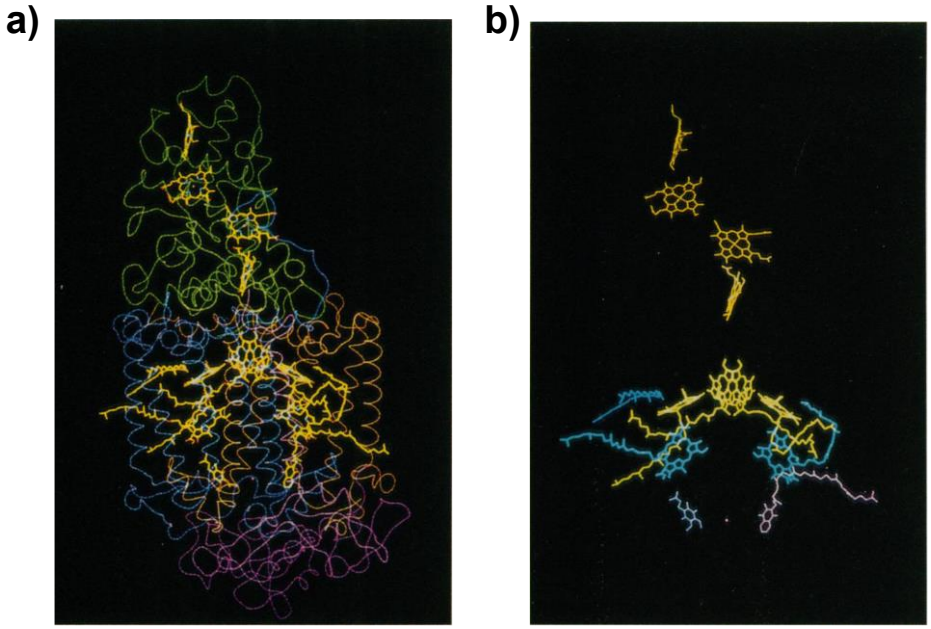

Fig. 1-2. (a) Overall view of the reaction center structure of purple photosynthesis bacterium and (b) the electron donor and acceptor molecules embedded in this reaction center.[37]

Sophisticated structural organization finds echoes in the photosynthetic systems of other lifebeings.[39–41] The high efficiency and precision observed in photoinduced electron transfer within natural photosynthesis serve as a crucial blueprint for creating artificial systems, particularly in the realm of solar energy conversion. Replicating these intricate natural processes within artificial settings presents a significant challenge yet promises sustainable and efficient solutions for harnessing solar energy. The comprehension of the foundational principles governing natural electron transfer is pivotal in guiding the development of artificial photosynthesis systems.

1-3. From nature to artificial: advances in artificial photoinduced electron transfer systems

In the quest to mimic natural photosynthesis, significant attention has been focused on developing artificial photoinduced electron transfer systems.[42–47] These efforts aim to replicate the fundamental process of natural photosynthesis - the transfer of electrons triggered by light absorption - in a controlled, artificial setting. The development of these artificial systems centers around establishing systems capable of effectively absorbing light and facilitating electron transfer.

1-3.1. Covalent and non-covalent linked electron transfer systems

The evolution of artificial photoinduced electron transfer systems has branched into two approaches: covalent and non-covalent linked systems. Both strategies are inspired by the intricate mechanisms observed in natural photosynthesis but differ in their assembly and functioning.[47]

Covalent electron transfer systems establish enduring, structured pathways for electron transmission within chemical bonds. This methodology affords meticulous regulation of distances and orientations between electron donors and acceptors, which is pivotal for optimizing the efficacy of electron transfer. [47–53]

Within covalent electron transfer systems, molecules serving as electron donors and acceptors are commonly interconnected via a 'bridge'. These 'bridges' encompass a spectrum of structures, including simple alkyl chains, oligomers, π-conjugated

architectures, DNA helices, and numerous other flexible or rigid frameworks.[54–61] The electron transfer occurring between the donor and acceptor molecules connected through this diverse array of 'bridges' has been extensively investigated. Some typical covalent systems are shown in Figs. 1-3–1-5.[55,56,61]

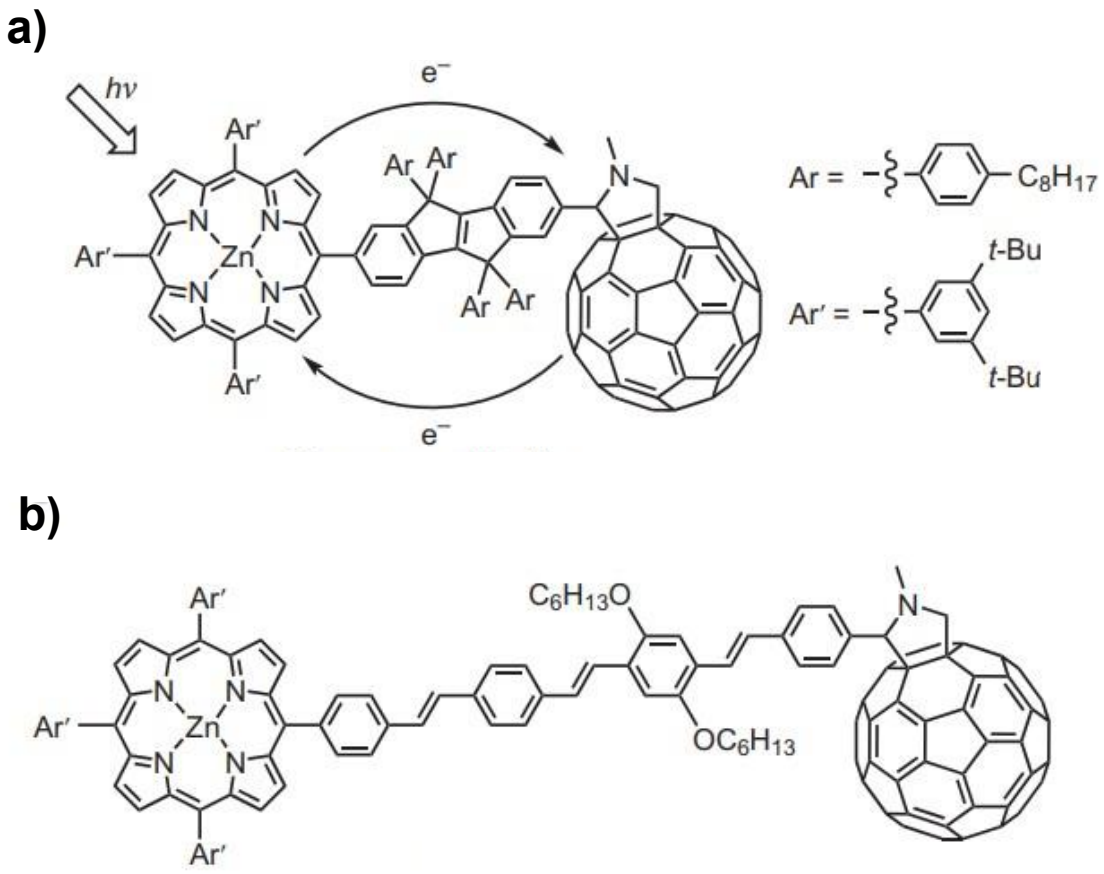

Fig. 1-3. Covalent electron transfer systems containing porphyrin and fullerene derivatives as electron donor and acceptor, linked by (a) a rigid molecular wire and (b) a flexible molecular wire.[55]

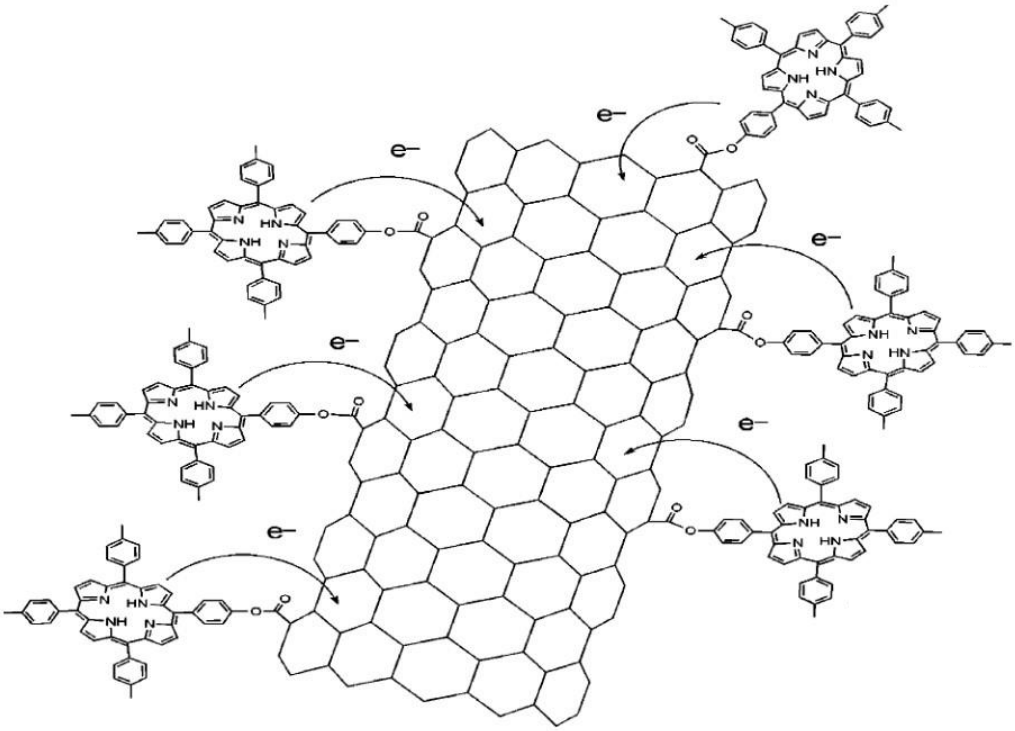

Fig. 1-4. A covalent electron transfer system consisting of porphyrins as electron donors and a carbon nanotube as electron accpetor.[56]

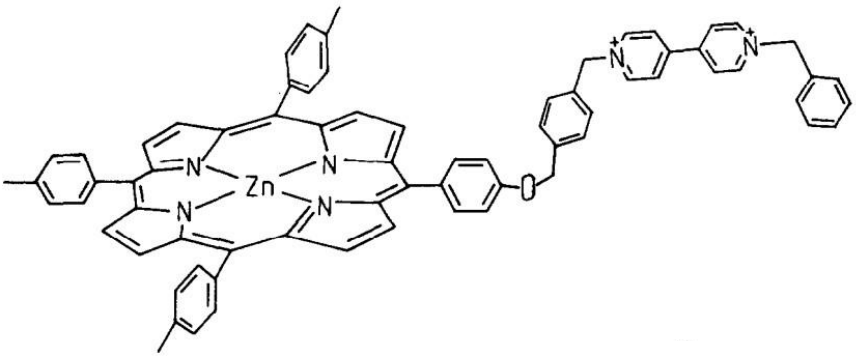

Fig. 1-5. A covalent electron transfer system consisting of a zinc porphyrin as electron donor and a viologen as electron accpetor.[61]

Non-covalent systems, also known as supramolecular systems, hinge on weaker yet versatile interactions such as hydrogen bonding, coordination bonding, van der Waals forces, and electrostatic interactions.[62–76] This characteristic grants them exceptional flexibility and the ability to self-assemble into intricate architectures, closely mimicking the dynamic nature of natural photosynthetic systems. Some typical supramolecular systems are shown in Figs. 1-6–1-8.[71,72,76]

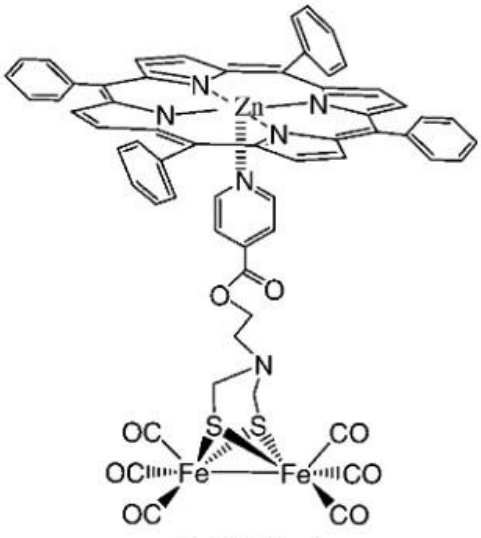

Fig. 1-6. A supramolecular electron transfer system formed by coordination bonding between a zinc porphyrin donor and a pyridyl bearing iron catalyst.[71]

Notably, our group previously established a supramolecular electron transfer system formed by host-guest interaction between a porphyrin donor and a cyclodextrin bearing a viologen acceptor (Fig. 1-7) and an efficient fluorescence quenching was observed in this system.[72]

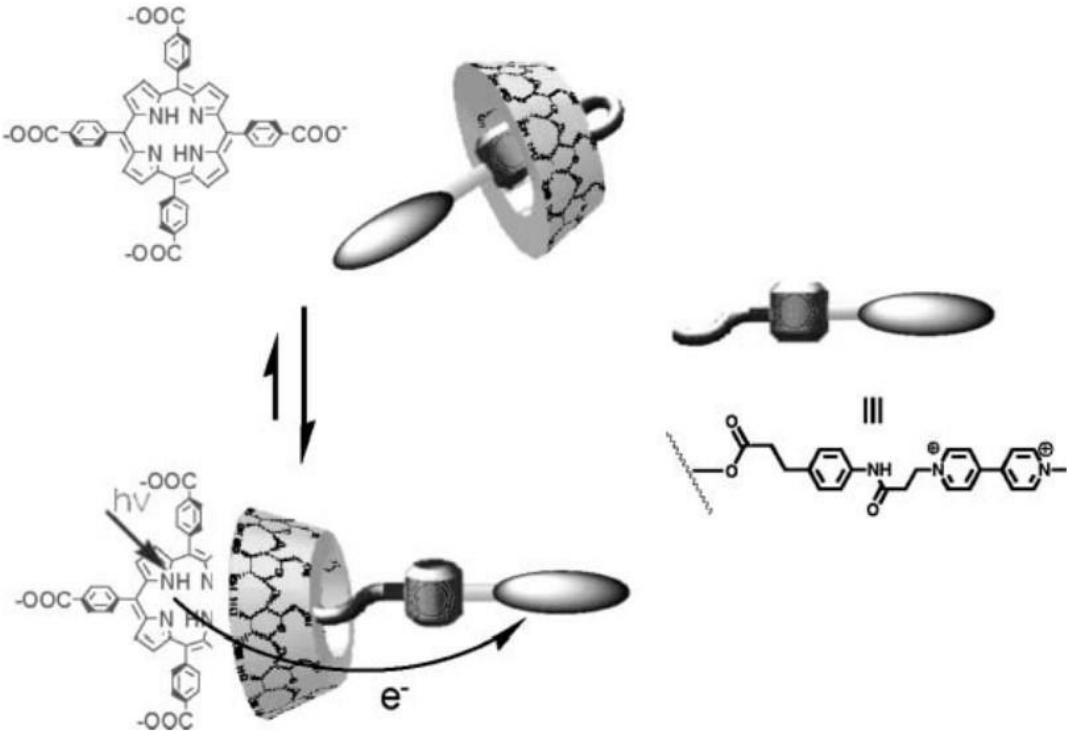

Fig. 1-7. A supramolecular electron transfer system formed by host-guest interaction between a porphyrin donor and a cyclodextrin bearing a viologen acceptor.[72]

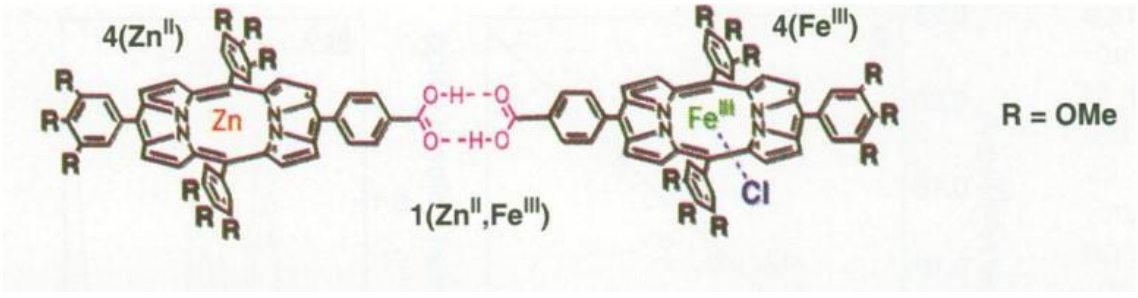

Fig. 1-8. A supramolecular electron transfer system formed by hydrogen bonding between a zinc porphyrin donor and an iron porphyrin acceptor.[76]

The capacity of supramolecular electron transfer systems for adaptation to diverse

conditions underscores their relevance in artificial photoinduced electron transfer.

1-3.2. Artificial photoinduced electron transfer systems within in polymer matrices

Investigating photoinduced electron transfer systems within polymer matrices signifies the forefront of foundational research, offering insights into intricate molecular interactions and energy transduction mechanisms. These systems serve as a platform to unravel fundamental principles governing electron transfer phenomena in controlled environments.[77] Their distinctiveness lies in embedding photoactive species within the polymer matrices, resembling the sophisticated structure found in the natural photosynthetic centers, thereby providing a refined environment for photoinduced electron transfer.

Research efforts predominantly concentrate on material selection and structural manipulation to create optimized situations for photoinduced electron transfer.[78–85]

Early research includes the covalently linkage of electron donor to polymer structures.[84,85] Morishima et. al. reported a zinc porphyrin–methylviologen electron transfer system, in which zinc porphyrins, as side chain pendants, are compartmentalized in unimer micelles (Fig. 1-9).[84] In such electron donor molecules covalently linked to polymer structures systems, over strong steric protections of polymers make electron acceptors and sacrificial agents hard to approach electron donors, which is unfavorable for photoinduced electron transfer.

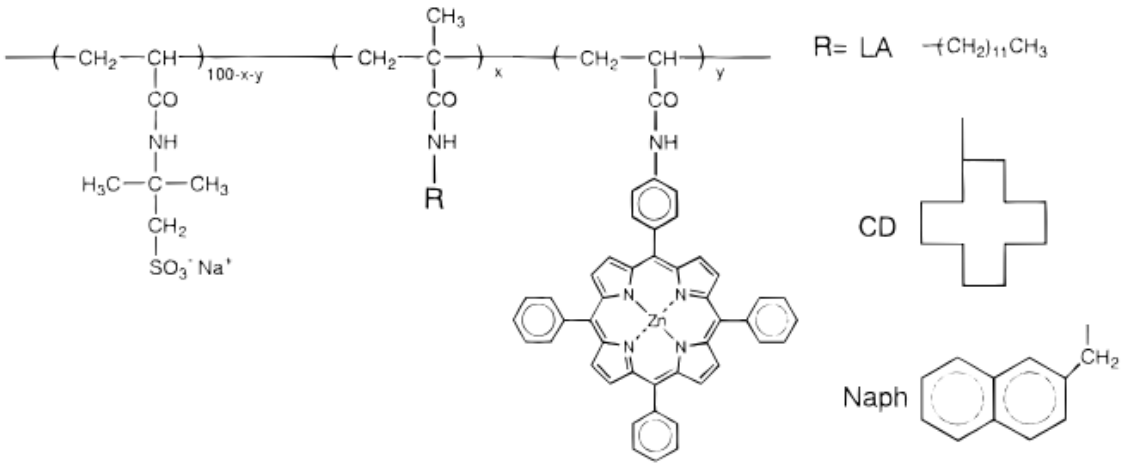

Fig. 1-9. Zinc porphyrin bearing terpolymers.[84]

Comparing to covalent linkage, using supramolecular interactions can provide a more flexible microenvironment for electron transfer. Our group previously reported that the photoinduced electron transfer from zinc porphyrin to methylviologen (MV^{2+}) was controlled by the complexation of monoclonal and zinc porphyrin (Fig. 1-10).[82] Recently, Shi et. al. reported a porphyrin–fullerene donor–acceptor system through a electrostatic self-assembling strategy in poly(ethylene glycol)-*b*-poly(L-lysine) polymer micelle, which serves as a shelter to prevent proton invasion, with high electron transfer efficiency (Fig. 1-11).[78]

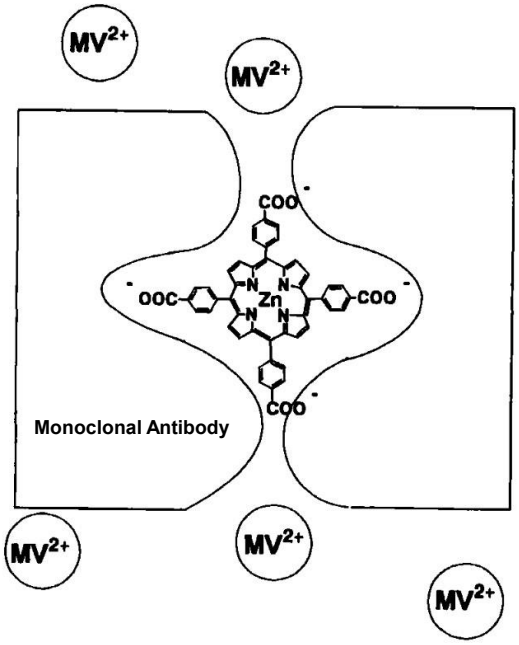

Fig. 1-10. A porphyrin-methylviologen electron transfer system built in monoclonal antibody matrix.[82]

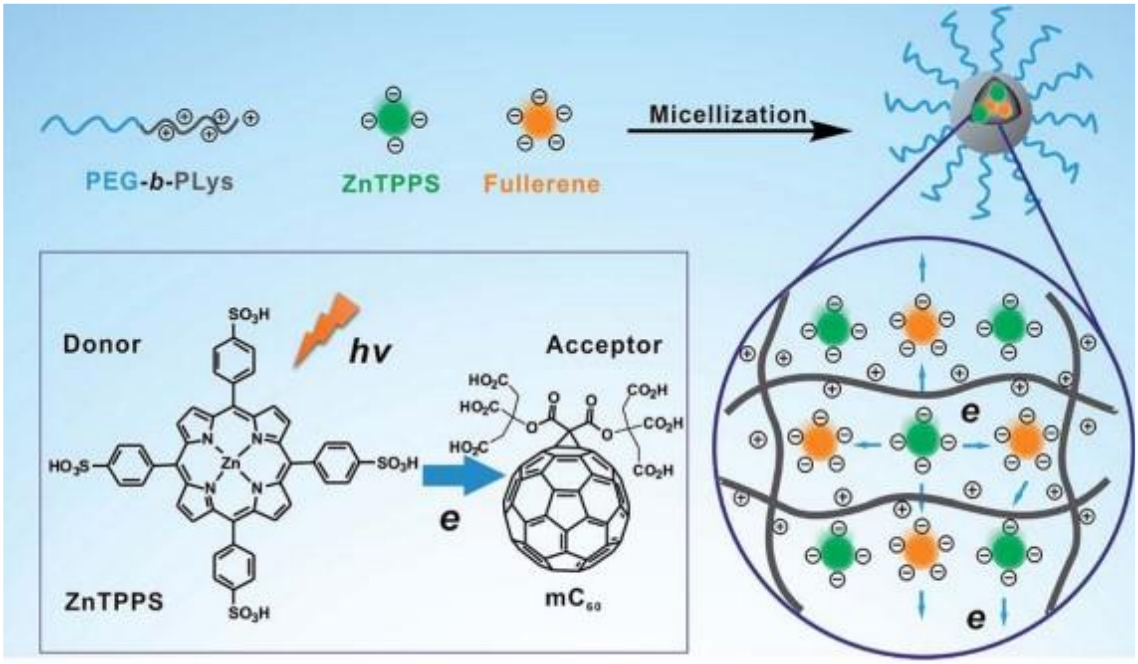

Fig. 1-11. A porphyrin-fullerene electron transfer system built in polymer micell.[78]

The similarity between these systems in polymer matrices and natural photosynthetic centers underscores their potential to provide a controlled environment for scrutinizing fundamental charge transfer phenomena, mirroring the intricate architecture observed in natural processes. This fundamental exploration within polymer matrices not only enriches our understanding of electron transfer dynamics but also offers a pathway for novel methodologies in artificial photosynthesis.

1-4. Scope and outline of this thesis

The central focus of this thesis revolves around the investigation and enhancement of artificial photoinduced electron transfer systems, specifically directing attention towards refining and comprehending mechanisms in supramolecular electron transfer systems within polymer matrices.

In Chapter 2, polyvinylpyrrolidone (PVP) was found to form complex with 5,10,15,20-tetrakis-(4-sulfonatophenyl)porphyrin (TPPS) and its zinc complex (ZnTPPS) quantitatively through different interactions (hydrogen bonds and coordination bonds, respectively). The formation of these complexes hinders the interaction between ground-state TPPS or ZnTPPS and an electron acceptor (methyl viologen, MV^{2+}) and can control the photoinduce electron transfer from TPPS or ZnTPPS to MV^{2+}, giving a larger amount of the electron transfer product, i. e. methyl viologen cationic radical ($MV^{+\bullet}$) (Fig. 1-12).

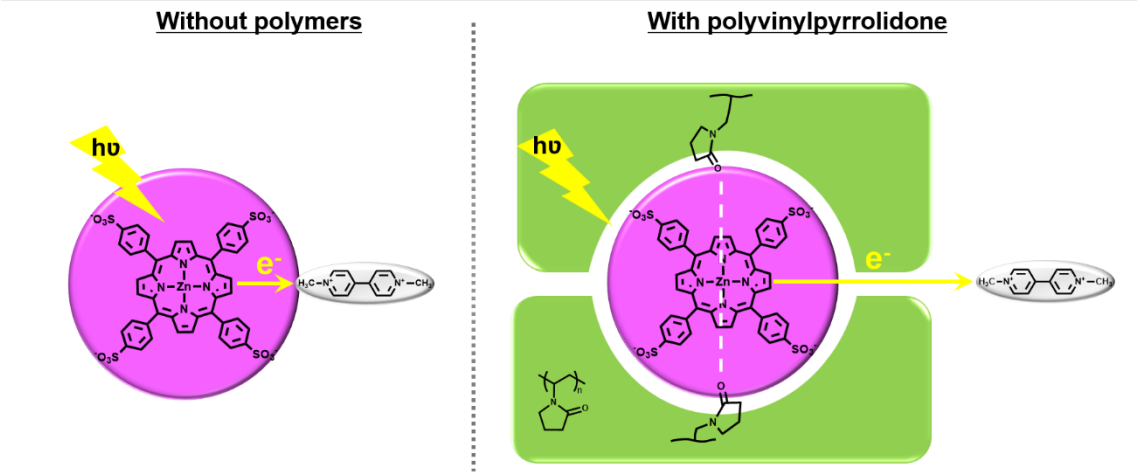

Fig. 1-12. Conceptual figure of ZnTPPS-MV^{2+} electron transfer system, set apart from and within the PVP polymer matrix.

In Chapter 3, an artificial photoinduced electron transfer system within a poly(*N*-methyl-4-vinylpyridinium) (P4VPMe) polymer matrix was developed. This system features TPPS and ZnTPPS as electron donors and MV^{2+} as the electron acceptor. In the presence of excess P4VPMe, ZnTPPS are molecularly dispersed rather than self-aggregating, favoring photoinduced electron transfer. Under these conditions, P4VPMe inhibits the formation of ground-state charge-transfer complex between ZnTPPS and MV^{2+}. This switches the main electron transfer process from singlet to triplet states. ZnTPPS in an excess of P4VPMe demonstrates over a tenfold increase in catalytic activity for the photoinduced oxidation of MV^{2+} compared to ZnTPPS alone (Fig. 1-13).

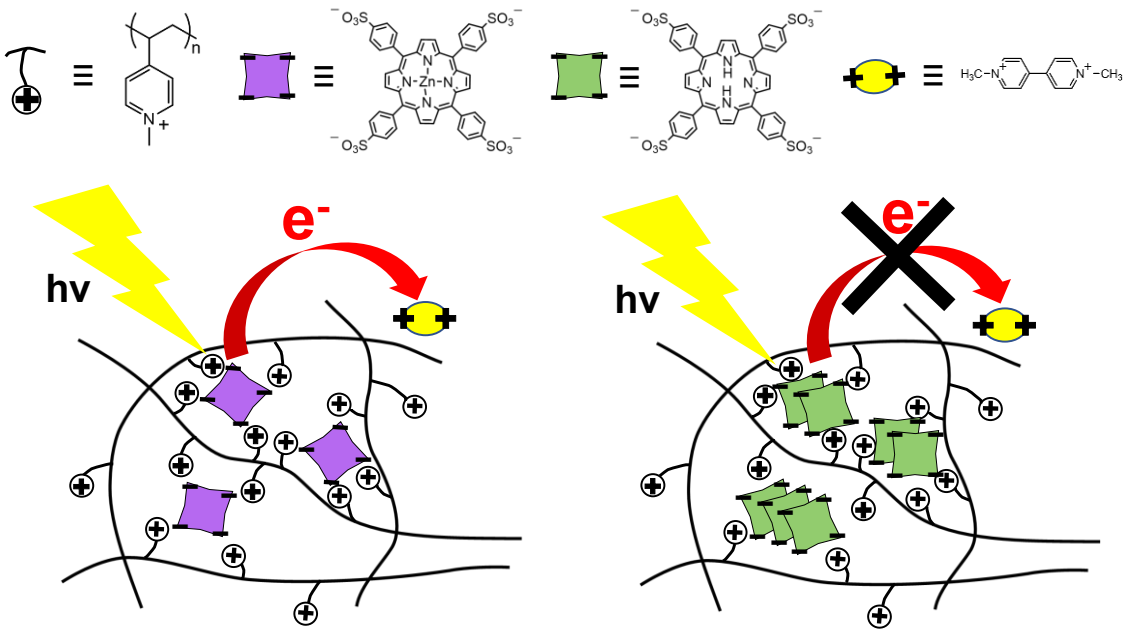

Fig. 1-13. Conceptual illustration depicting ZnTPPS molecules individually dispersed within the P4VPMe polymer matrix, facilitating photoinduced electron transfer, contrasted with TPPS aggregates within the same matrix, unfavorable for such electron transfer.

In Chapter 4, works presented in Chapter 2 and Chapter 3 are summarized.

References

1. Abas, N.; Kalair, A.; Khan, N. *Futures* **2015**, *69*, 31-49.
2. Bhattarai, K.; Stalick, W.; Mckay, S.; Geme, G.; Bhattarai, N. *J. Environ. Sci. Health Part A Toxic/Hazard. Subst. Environ. Eng.* **2011**, *46*, 1424-1442.
3. Lackner, K.; Hester, R.; Harrison, R. *Carbon Capture: Sequestration and Storage* **2010**, *29*, 1-40.
4. Peter, S. *ACS Energy Lett.* **2018**, *3*, 1557-1561.
5. Lewis, N.; Nocera, D. *Proc. Natl. Acad. Sci. U.S.A.* **2006**, *103*, 15729-15735.
6. Hayat, M.; Ali, D.; Monyake, K.; Alagha, L.; Ahmed, N. *Int. J. Energy Res.* **2019**, *43*, 1049-1067.
7. Kabir, E.; Kumar, P.; Kumar, S.; Adelodun, A.; Kim, K. *Renew. Sustain. Energy Rev.* **2018**, *82*, 894-900.
8. Kannan, N.; Vakeesan, D. *Renew. Sustain. Energy Rev.* **2016**, *62*, 1092-1105.
9. Kalair, A.; Abas, N.; Saleem, M.; Kalair, A.; Khan, N. *Energy Storage* **2021**, *3*.
10. York, R.; Bell, S. *Energy Res. Soc. Sci.* **2019**, *51*, 40-43.
11. Moran, E.; Lopez, M.; Moore, N.; Müller, N.; Hyndman, D. *Proc. Natl. Acad. Sci. U.S.A.* **2018**, *115*, 11891-11898.
12. Leung, D.; Yang, Y. Renew. *Sustain. Energy Rev.* **2012**, *16*, 1031-1039.
13. Demain, A. *J. Ind. Microbiol. Biotechnol.* **2009**, *36*, 319-332.
14. Barber, J.; Tran, P. *J. R. Soc. Interface* **2013**, *10*.
15. McConnell, I.; Li, G.; Brudvig, G. *Chem. Biol.* **2010**, *17*, 434-447.
16. Barber, J. *Chem. Soc. Rev.* **2009**, *38*, 185-196.
17. Hohmann-Marriott, M.; Blankenship, R.; Merchant, S.; Briggs, W.; Ort, D. *Annu. Rev. Plant Biol.* **2011**, *62*, 515-548.

18. Krause, G.; Weis, E. *Annu. Rev. Plant Physiol. Plant Mol. Biol.* **1991**, *42*, 313-349.

19. Li, X.; Lei, H.; Xie, L.; Wang, N.; Zhang, W.; Cao, R. *Acc. Chem. Res.* **2022**, *55*, 878-892.

20. Fukuzumi, S.; Honda, T.; Kojima, T. *Coord. Chem. Rev.* **2012**, *256*, 2488-2502.

21. Wasielewski, M. *Acc. Chem. Res.* **2009**, *42*, 1910-1921.

22. Fukuzumi, S.; Fujioka, N.; Kotani, H.; Ohkubo, K.; Lee, Y.; Nam, W. *J. Am. Chem. Soc.* **2009**, *131*, 17127-17134.

23. Claessens, C.; Hahn, U.; Torres, T. *Chem. Rec.* **2008**, *8*, 75-97.

24. D'Souza, F.; Ito, O. *Coord. Chem. Rev.* **2005**, *249*, 1410-1422.

25. Leister, D. *Mol. Plant* **2023**, *16*, 4-22.

26. Emerson, R.; Arnold, W. *J. Gen. Physiol.* **1932**, *16*, 191-205.

27. Shimizu, R.; Dempo, Y.; Nakayama, Y.; Nakamura, S.; Bamba, T.; Fukusaki, E.; Fukui, T. *Sci. Rep.* **2015**, *5*.

28. Firooznia, F. *Am. Biol. Teach.* **2007**, *69*, 364-367.

29. Melis, A. *Plant Sci.* **2009**, *177*, 272-280.

30. Vasil'ev, S.; Bruce, D. *Plant Cell* **2004**, *16*, 3059-3068.

31. Wang, Y.; Suzuki, H.; Xie, J.; Tomita, O.; Martin, D.; Higashi, M.; Kong, D.; Abe, R.; Tang, *J. Chem. Rev.* **2018**, *118*, 5201-5241.

32. Thilagam, A. *J. Math. Chem.* **2015**, *53*, 466-494.

33. Sayama, K.; Yoshida, R.; Kusama, H.; Okabe, K.; Abe, Y.; Arakawa, H. *Chem. Phys. Lett.* **1997**, *277*, 387–391.

34. Vinyard, D.; Ananyev, G.; Dismukes, G.; Kornberg, R. *Annu. Rev. Biochem.* **2013**, *82*, 577-606.

35. Rees, D.; Komiya, H.; Yeates, T.; Allen, J.; Feher, G. *Annu. Rev. Biochem.* **1989**, *58*,

607-633.

36. Deisenhofer, J.; Michel, H. *EMBO J.* **1989**, *8*, 2149-2170.
37. Deisenhofer, J.; Michel, H. *Science* **1989**, *245*, 1463-1473.
38. Michel, H.; Deisenhofer, *J. Biochemistry* **1988**, *27*, 1-7.
39. Xiong, J.; Bauer, C. *Annu. Rev. Plant Biol.* **2002**, *53*, 503-521.
40. Feher, G. A. J. P.; Allen, J. P.; Okamura, M. Y.; Rees, D. C. *Nature* **1989**, *339*, 111-116.
41. Thornber, J. Annu. Rev. *Plant Physiol. Plant Mol. Biol*. **1975**, *26*, 127-158.
42. Velasco-Garcia, L.; Casadevall, C. *Commun. Chem.* **2023**, *6*.
43. Wang, C.; O'Hagan, M.; Willner, B.; Willner, I. *Chem. Eur. J.* **2022**, *28*.
44. Fukuzumi, S.; Lee, Y.; Nam, W. *Tetrahedron* **2020**, *76*.
45. Fukuzumi, S. *Phys. Chem. Chem. Phys.* **2008**, *10*, 2283-2297.
46. Piotrowiak, P. *Chem. Soc. Rev.* **1999**, *28*, 143-150.
47. Wasielewski, M. *Chem. Rev.* **1992**, *92*, 435-461.
48. Bottari, G.; de la Torre, G.; Guldi, D.; Torres, T. *Chem. Rev.* **2010**, *110*, 6768-6816.
49. Roncali, *J. Chem. Soc. Rev.* **2005**, *34*, 483-495.
50. El-Khouly, M.; Ito, O.; Smith, P.; D'Souza, F. *J. Photochem. Photobiol. C-Photochem. Rev.* **2004**, *5*, 79-104.
51. Imahori, H. *Org. Biomol. Chem.* **2004**, *2*, 1425-1433.
52. Imahori, H.; Sakata, Y. *Adv. Mater.* **1997**, *9*, 537.
53. Murphy, C.; Arkin, M.; Jenkins, Y.; Ghatlia, N.; Bossmann, S.; Turro, N.; Barton, J. *Science* **1993**, *262*, 1025-1029.
54. Sukegawa, J.; Schubert, C.; Zhu, X.; Tsuji, H.; Guldi, D.; Nakamura, E. *Nat. Chem.* **2014**, *6*, 899-905.

55. Sukegawa, J.; Schubert, C.; Zhu, X.; Tsuji, H.; Guldi, D.; Nakamura, E. *Nat. Chem.* **2014**, *6*, 899-905.

56. Baskaran, D.; Mays, J.; Zhang, X.; Bratcher, M. *J. Am. Chem. Soc.* **2005**, *127*, 6916-6917.

57. Weiss, E. A. et al. *J. Am. Chem. Soc.* **2004**, *126*, 5577–5584.

58. Imahori, H.; Yamada, H.; Guldi, D.; Endo, Y.; Shimomura, A.; Kundu, S.; Yamada, K.; Okada, T.; Sakata, Y.; Fukuzumi, S. *Angew. Chem. Int. Ed.* **2002**, *41*, 2344-2347.

59. Kelley, S.; Barton, J. *Science* **1999**, *283*, 375-381.

60. Davis, W.; Svec, W.; Ratner, M.; Wasielewski, M. *Nature* **1998**, *396*, 60-63.

61. Levin, P.; Batova, E.; Shafirovich, V. *Chem. Phys.* **1990**, *142*, 279-289.

62. Ham, R.; Nielsen, C.; Pullen, S.; Reek, *J. Chem. Rev.* **2023**, *123*, 5225-5261.

63. Xu, Y.; Wang, B.; Kaur, R.; Minameyer, M.; Bothe, M.; Drewello, T.; Guldi, D.; von Delius, M. *Angew. Chem. Int. Ed.* **2018**, *57*, 11549-11553.

64. Kawashima, Y.; Ohkubo, K.; Fukuzumi, S. *Chem. Asian J.* **2015**, *10*, 44-54.

65. Frischmann, P.; Mahata, K.; Würthner, F. *Chem. Soc. Rev.* **2013**, *42*, 1847-1870.

66. Bottari, G.; Trukhina, O.; Ince, M.; Torres, T. *Coord. Chem. Rev.* **2012**, *256*, 2453-2477.

67. Fukuzumi, S.; Ohkubo, K.; D'Souza, F.; Sessler, J. *Chem. Commun.* **2012**, *48*, 9801-9815.

68. Sandanayaka, A.; Ito, O. *J. Porphyrins Phthalocyanines* **2009**, *13*, 1017-1033.

69. Wasielewski, M. *Acc. Chem. Res.* **2009**, *42*, 1910-1921.

70. Chitta, R.; D'Souza, F. *J. Mater. Chem.* **2008**, *18*, 1440-1471.

71. Li, X.; Wang, M.; Zhang, S.; Pan, J.; Na, Y.; Liu, J.; Åkermark, B.; Sun, L. *J. Phys. Chem. B* **2008**, *112*, 8198-8202.

72. Deng, W.; Onji, T.; Yamaguchi, H.; Ikeda, N.; Harada, A. *Chem. Commun.* **2006**, 4212-4214.

73. D'Souza, F.; Ito, O. *Coord. Chem. Rev.* **2005**, *249*, 1410-1422.

74. El-Khouly, M.; Ito, O.; Smith, P.; D'Souza, F. *J. Photochem. Photobiol. C-Photochem. Rev.* **2004**, *5*, 79-104.

75. Hayashi, T.; Ogoshi, H. *Chem. Soc. Rev.* **1997**, *26*, 355-364.

76. Derege, P.; Williams, S.; Therien, M. *Science* **1995**, *269*, 1409-1413.

77. D. Nocera, *Acc. Chem. Res.* **2012**, *45*, 767-776.

78. Wang, R.; Qu, R.; Jing, C.; Zhai, Y.; An, Y.; Shi, L. *RSC Adv.* **2017**, *7*, 10100-10107.

79. Krieger, A.; Werner, J.; Mariani, G.; Gröhn, F. *Macromolecules* **2017**, *50*, 3464-3475.

80. Frühbeisser, S.; Gröhn, F. *J. Am. Chem. Soc.* **2012**, *134*, 14267-14270.

81. Wang, X.; Zhao, L.; Ma, R.; An, Y.; Shi, L. *Chem. Commun.* **2010**, *46*, 6560-6562.

82. Harada, A.; Yamaguchi, H.; Okamoto, K.; Fukushima, H.; Shiotsuki, K.; Kamachi, M. *Photochem. Photobiol.* **1999**, *70*, 298-302.

83. Sadamoto, R.; Tomioka, N.; Aida, T. *J. Am. Chem. Soc.* **1996**, *118*, 3978-3979.

84. Aota, H.; Araki, S. I.; Morishima, Y.; Kamachi, M. *Macromolecules* **1997**, *30*, 4090–4096.

85. Morishima, Y.; Itoh, Y.; Nozakura, S.; Ohno, T.; Kato, S. *Macromolecules* **1984**, *17*, 2264–2269.

Chapter 2

Control of Photoinduced Electron Transfer Using Complex Formation of Water-Soluble Porphyrin and Polyvinylpyrrolidone

2-1. Introduction

Given the depletion of fossil fuel reserves and escalating environmental concerns, the imperative development and adoption of sustainable energies like solar, wind, water, and biomass energy has gained paramount importance.[1,2] Among these, solar energy stands as the most abundant and consistent resource available on Earth.[3] Nature exemplifies the optimum utilization of solar energy. Natural photosynthetic systems demonstrate remarkable efficiency in converting solar energy into chemical energy.[4] Central to these systems are the pigments within photosynthetic reaction centers, ensconced by surrounding proteins. This arrangement ensures the non-covalent fixation of electron donors and acceptors at an optimal distance and relative position, facilitating efficient electron transfer.[4–9]

Extensive endeavors have been directed towards emulating the natural photosynthetic systems to explore the initial processes of photosynthesis and realize highly efficient electron transfer in artificial systems.[10–27] Studies investigating electron transfer systems through covalently linked donor-acceptor molecules have been well-documented.[10–13] Recent advancements have introduced covalently linked donor-acceptor systems, notably utilized as photoinitiators in polymerization processes.[14,15] Additionally, non-covalent assemblies of electron donor and acceptor molecules have been established, employing

mechanisms such as hydrogen bonding,[16–18] metal coordination,[18–20] electrostatic interaction,[21–23] and host–guest interaction.[24–27] Among these investigations, those employing polymer matrices have garnered substantial interest, owing to their ability to immobilize electron donors, mimicking the natural photosynthetic systems. Notably, Aida et al. demonstrated the use of porphyrin dendrimers to regulate electron transfer distance between porphyrin and methyl viologen.[21] Recently, Shi et al. reported controlled electron transfer between porphyrin and water-soluble fullerene within poly(ethylene glycol)-block-poly(l-lysine) micelles.[23] However, the intricate molecular design and synthesis processes still present challenges, warranting the development of a more convenient and generalized approach.

In this study, polyvinylpyrrolidone (PVP, Fig. 2-1) was observed to form complexes with 5,10,15,20-tetrakis-(4-sulfonatophenyl) porphyrin (TPPS, Fig. 2-1) and its zinc complex (ZnTPPS, Fig. 2-1) through various interactions. Here, the author presents a discovery that the interaction between porphyrins and the electron acceptor, methyl viologen (MV^{2+}, Fig. 2-1), can be modulated in the presence of PVP, resulting in an amplified concentration of electron-transfer products.

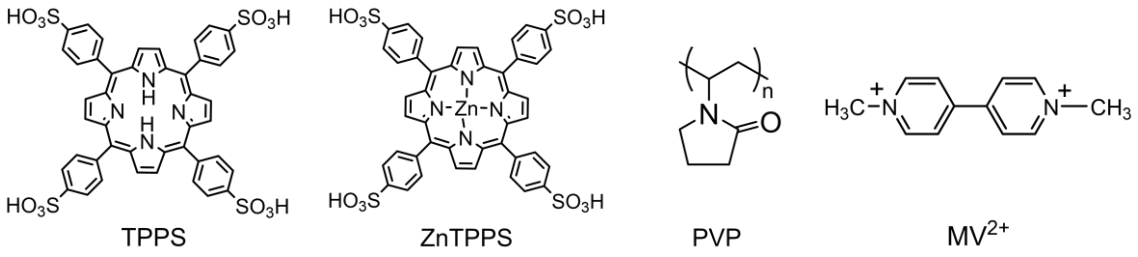

Fig. 2-1. Chemical structures of TPPS, ZnTPPS, PVP and MV^{2+}.

2-2. Materials and Methods

Materials

Tetraphenylporphyrin tetrasulfonic acid hydrate (TPPS) and polyethylene glycol 6000 (PEG 6000) were acquired from TCI Co., Ltd., Tokyo, Japan. Polyvinylpyrrolidone (PVP 25 (M = 24,500), K-30 (M = 40,000), and K-90 (M = 360,000), M represents for the average molecular weight), methyl viologen hydrate, potassium dihydrogenphosphate, dipotassium hydrogenphosphate, and ethylenediamine-*N,N,N′,N′*-tetraacetic acid tetrasodium salt (EDTA) were purchased from Nacalai Tesque, Kyoto, Japan. All reagents and solvents were used as received without further purification. Zinc *meso*-5,10,15,20-tetrakis-(4-sulfonatophenyl)porphyrin (ZnTPPS) was synthesized according to the method reported by Flamigni et al.[28]

Methods

The ^{1}H NMR spectra were acquired using a JEOL (Tokyo, Japan) JNM-ECA 500 MHz NMR spectrometer. Chemical shifts were referenced to sodium 3-(trimethylsilyl)-1-propanesulfonate (δ = 0.00 ppm) and the solvent value (δ = 4.79 ppm for D_2O). UV–vis spectra were recorded on a SHIMADZU (Kyoto, Japan) UV-2500PC spectrophotometer at 25 °C using a cell with a 1 cm path length. Fluorescence spectra were recorded on a HITACHI F-2500 fluorescence spectrophotometer (Tokyo, Japan). Slit widths were both 5.0 nm for excitation and emission side and sensitivity was set to high. Raman scattering of the ZnTPPS in the absence and presence of PVP or pyridine was excited by ~20 ns

laser pulses of 425 nm generated using the second harmonic of a Ti:sapphire laser pumped by a Q-switched diode-pumped Nd-doped yttrium lithium fluoride (Nd:YLF) laser (TU-L, Photonics Industries, Ronkonkoma, NY, USA) at 1 kHz. The pulse energy at the sample was 0.5 μJ. The sample solution was placed in a glass tube used as a spinning cell, and the scattered Raman light was collected and focused onto the entrance slit of a spectrograph (iHR550, HORIBA Jobin Ybon, Kyoto, Japan) equipped with a charge-coupled-device (CCD) camera (SPEC-10:400B/LN-SN-U, Roper Scientific, Sarasota, FL, USA). The accumulation times for obtaining each spectrum were 5 min. The Raman shifts were calibrated using the Raman bands of cyclohexane. The calibration error was within 1 cm^{-1} for prominent bands. Irradiation experiments were carried out using a UV irradiation unit (SP-11, USHIO, Tokyo, Japan) equipped with an ND10 filter (HOYA, Tokyo, Japan).

2-3. Results and Discussion

2-3.1. Formation of Complexes

We investigated the interaction between ZnTPPS and PVP (refers to PVP K-30 unless otherwise noted) in a 0.01 M phosphate buffer at pH 8.0. Upon the addition of PVP, noticeable redshifts appeared in the Soret band (Fig. 2-2a) and the Q-bands (Fig. 2-3) of ZnTPPS. These spectral shifts indicate the formation of a complex between ZnTPPS and PVP.

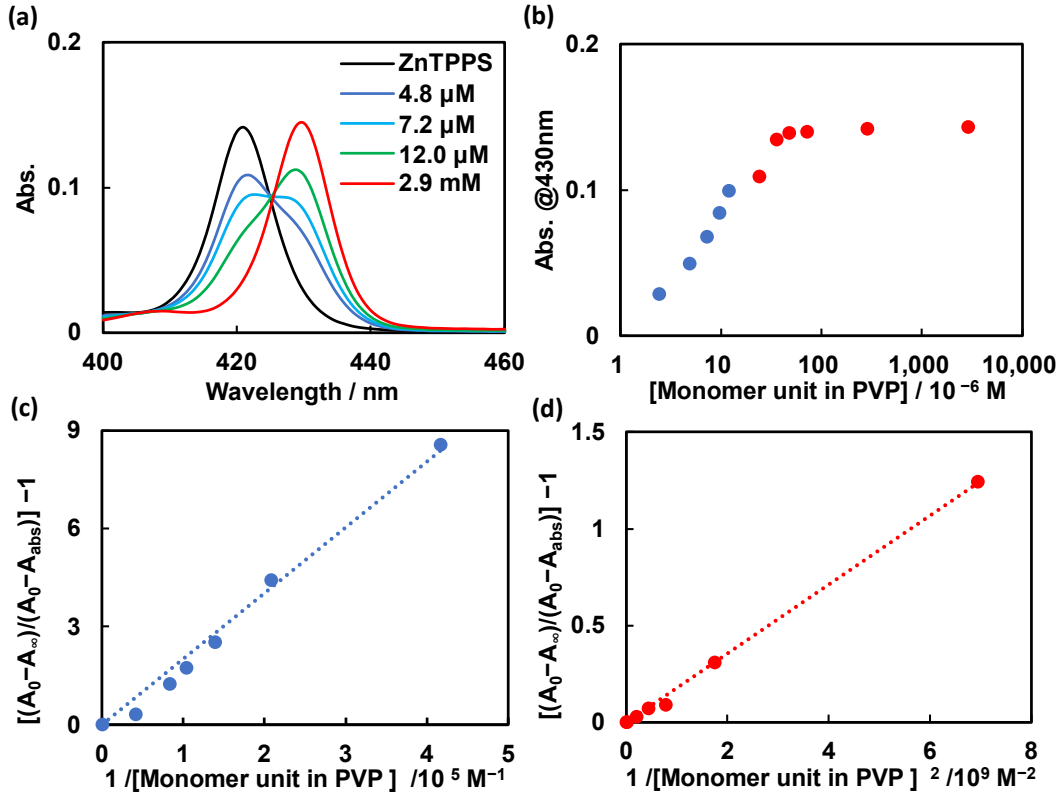

Fig. 2-2. (a) Absorption spectra of ZnTPPS upon the addition of PVP at Soret band in 0.01 M phosphate buffer (pH 8.0); (b) A plot of Abs. at 430 nm as a function of the concentration of PVP; BH plots for the formation of ZnTPPS–PVP complex under the assumption of the formation of (c) a 1:1 complex and (d) a 1:2 complex in the lower and higher PVP concentration regions, respectively.

Benesi–Hildebrand (BH) plots,[29] based on the absorbance at 430 nm (Fig. 2-2b), were generated to ascertain the molar ratio of ZnTPPS and PVP monomer unit in a complex and association constant of the ZnTPPS–PVP complex. The BH plots for 1:1 and 1:2 complex formation ratios, observed in low and high PVP concentration ranges, respectively, are depicted in Figs. 2-2c and 2-2d. Both plots exhibited linearity within their respective PVP concentration ranges, indicating the formation of ZnTPPS–PVP complexes in a 1:1 (ZnTPPS:PVP monomer unit) and 1:2 ratio in lower and higher PVP

concentration regions, respectively. The association constants were determined from the slopes and computed as $K_{1,\mathrm{ZnTPPS}} = 5.0 \times 10^4\ \mathrm{M}^{-1}$ and $K_{1,\mathrm{ZnTPPS}} \times K_{2,\mathrm{ZnTPPS}} = 5.0 \times 10^9\ \mathrm{M}^{-2}$ ($K_{1,\mathrm{ZnTPPS}}$ and $K_{2,\mathrm{ZnTPPS}}$ are the first and second binding constants of ZnTPPS with PVP, respectively).

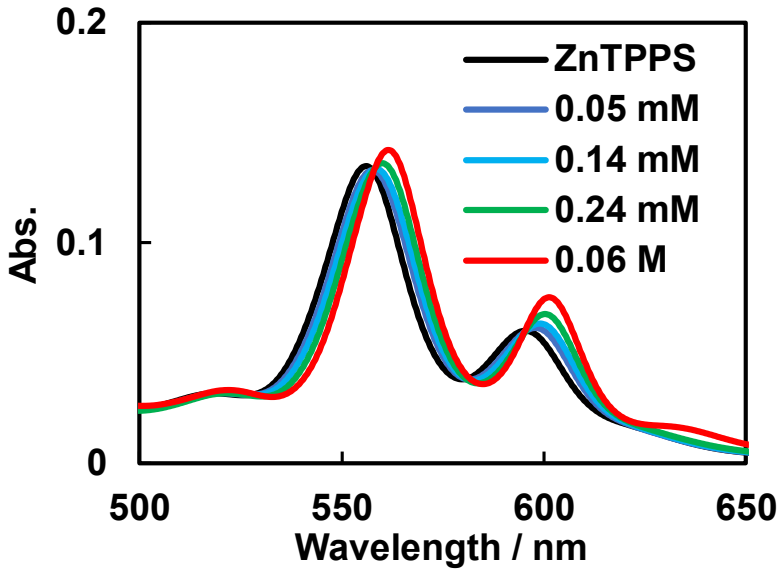

Fig. 2-3. Absorption spectra of ZnTPPS upon the addition of PVP at Q-bands in 0.01 M phosphate buffer (pH 8.0).

In addition to the observed redshifts in the absorption spectra of ZnTPPS (12.0 μM), a distinct color change from purple to green was also noted (Fig. 2-4). Both alterations are typical when an agent interacts with zinc porphyrin via a coordination bond.[30–32]

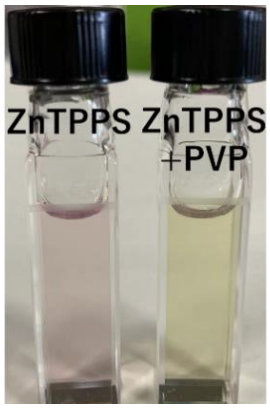

Fig. 2-4. Color change of ZnTPPS solution upon the addition of PVP.

Our hypothesis centered on the formation of a ZnTPPS–PVP complex via a coordination bond between the carbonyl group of PVP and the central Zn atom of ZnTPPS (Fig. 2-8a). This interpretation finds support from the ^{1}H NMR spectra (Fig. 2-5) and Raman spectra (Fig. 2-6).

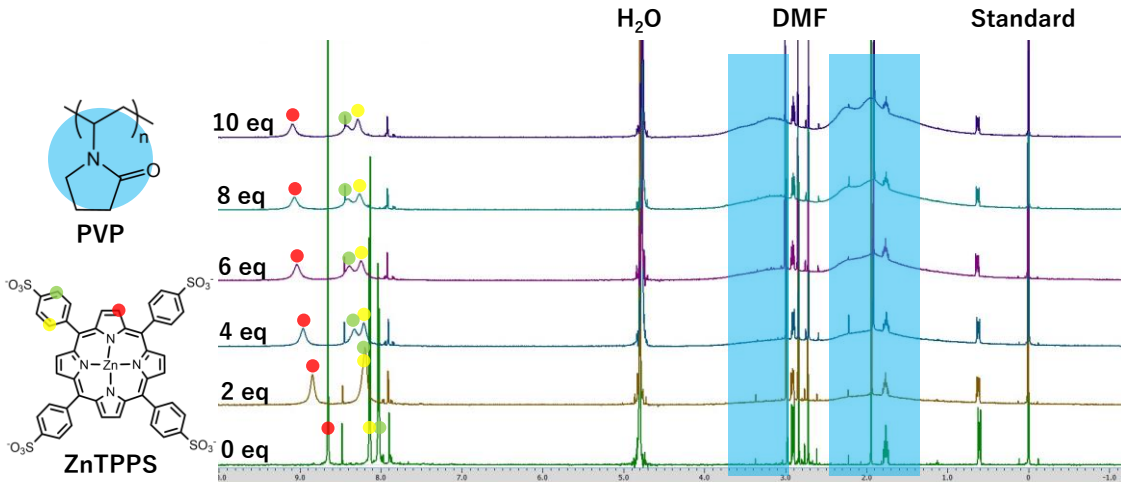

Fig. 2-5. ^{1}H NMR spectra of mixing solutions of ZnTPPS and PVP, in D_2O at 25°C.

The chemical shifts of the protons on the pyrrole rings exhibited the largest shifts (Fig. 2-5), suggesting that PVP interacts with ZnTPPS at the center of the porphyrin ring.

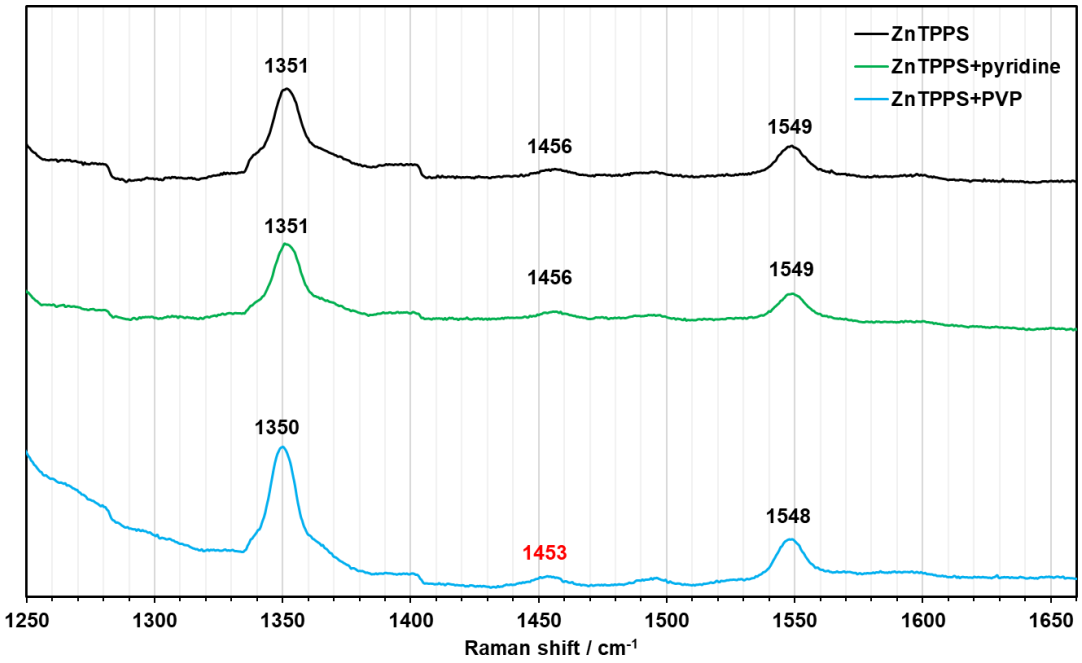

Fig. 2-6. Raman spectra of mixing solutions of ZnTPPS and PVP or pyridine.

The Raman band near 1,450 cm^{-1} showed a 3 cm^{-1} downshift in the presence of PVP, whereas no shifts were observed upon the addition of pyridine (Fig. 2-6). The frequency of this band is sensitive to the spin state (or coordination number) of the porphyrin. The observed downshift indicated that the high-spin character of the porphyrin increased in the presence of PVP. We speculated that PVP interacts with ZnTPPS through a coordination bond between the carbonyl groups of PVP and the central zinc atom of ZnTPPS.

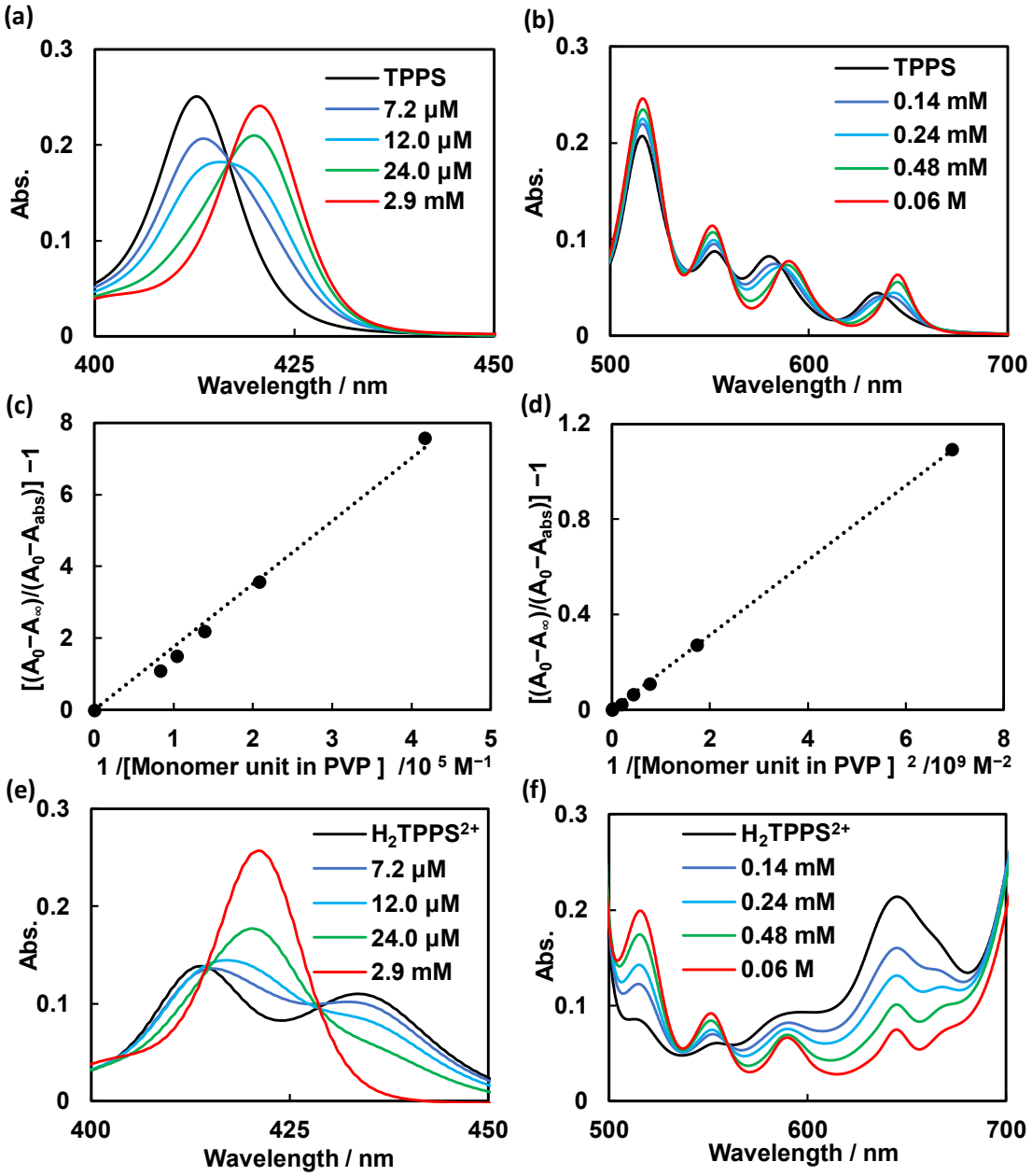

Fig. 2-7. Absorption spectra of TPPS upon the addition of PVP at (a) Soret band and (b) Q-bands in 0.01 M phosphate buffer (pH 8.0); BH plots for the formation of a TPPS–PVP complex under the assumption of the formation of (c) a 1:1 complex and (d) a 1:2 complex in the lower and higher PVP concentration regions, respectively; Absorption spectra of H_2TPPS^{2+} upon the addition of PVP at (e) Soret band and (f) Q-bands in 0.01 M phosphate buffer (pH 4.0).

The absorption spectra of TPPS, both in the presence and absence of PVP, were recorded in 0.01 M phosphate buffer (pH = 8.0). Notable redshifts in the Soret band and Q-bands (Figs. 2-7a and 2-7b) strongly indicate the formation of a TPPS–PVP complex. Corresponding BH plots were constructed similarly to those for the ZnTPPS–PVP complex (Figs. 2-7c and 2-7d). The BH plots indicate the formation of the TPPS–PVP complex at ratios of 1:1 (TPPS:PVP monomer unit) and 1:2 in the lower and higher PVP concentration regions, respectively. The association constants were evaluated to be $K_{1,\mathrm{TPPS}} = 5.0 \times 10^4\ \mathrm{M}^{-1}$ and $K_{1,\mathrm{TPPS}} \times K_{2,\mathrm{TPPS}} = 5.0 \times 10^9\ \mathrm{M}^{-2}$ ($K_{1,\mathrm{TPPS}}$ and $K_{2,\mathrm{TPPS}}$ are the first and second binding constants of TPPS with PVP, respectively).

The interaction of protonated TPPS (H_2TPPS^{2+}) with PVP was also studied at pH 4, presenting a Soret band at 434 nm (Fig. 2-7e). The Q-bands appeared at 516, 553, 590 and 645 nm (Fig. 2-7f), with the Q_y absorption bands being more intense than the Q_x bands. Upon the introduction of PVP, the Soret band of H^2TPPS_{2+} shifted to 430 nm. This shift reversed the absorption pattern, resulting in slight shifts in the Q_y and Q_x bands until the Q-bands matched those in the spectrum of TPPS. Our interpretation suggests the formation of a TPPS–PVP complex facilitated by hydrogen bonding between the carbonyl group of PVP and the central amino group of TPPS (Fig. 2-8b), observed even under acidic pH conditions.

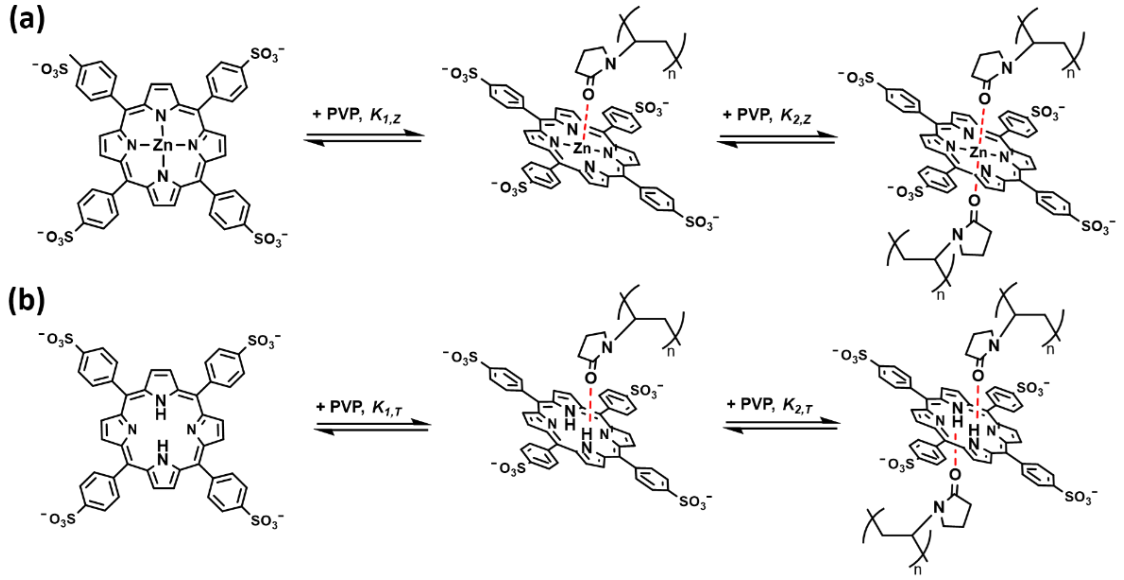

Fig. 2-8. Conceptual schemes of the formation of the (a) ZnTPPS–PVP complex and (b) TPPS–PVP complex.

The fluorescence intensity of both TPPS and ZnTPPS (Fig. 2-9) exhibited an increase upon the addition of PVP. This observation implies that the presence of PVP retards the themal quenching of the porphyrins, e.g. the collision of solvent molecules.[25,27]

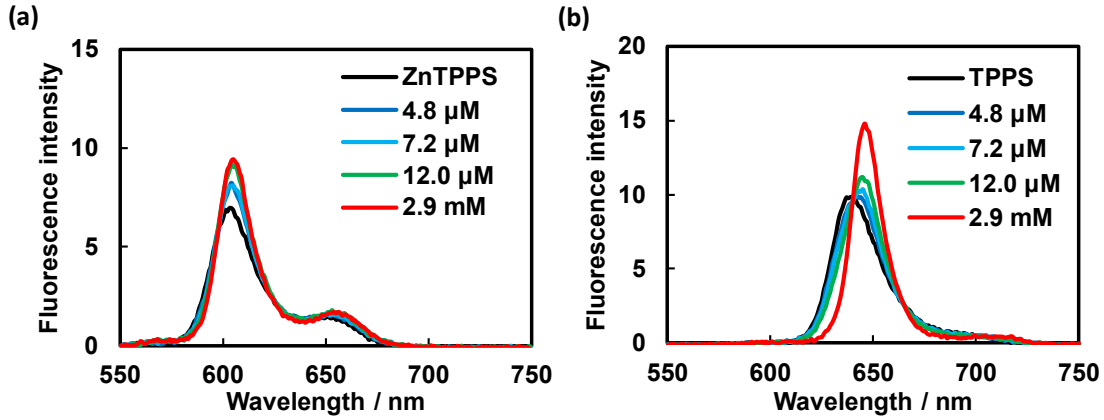

Fig. 2-9. Fluorescence spectra of (a) ZnTPPS (λ_{ex} = 425 nm) and (b) TPPS (λ_{ex} = 417 nm) upon the addition of PVP.

The absorption spectra of ZnTPPS or TPPS in the presence of *N*-methyl-2-pyrrolidone (NMP) (Figs. 2-10a and 2-10b) or *N*-vinyl-2-pyrrolidone (NVP) (Figs. 2-10c and -10d) suggest minimal interactions of NMP or NVP with ZnTPPS or TPPS. This underscores the critical importance of the steric effect imparted by the polymer structure of PVP in the formation of the ZnTPPS–PVP and TPPS–PVP complexes.

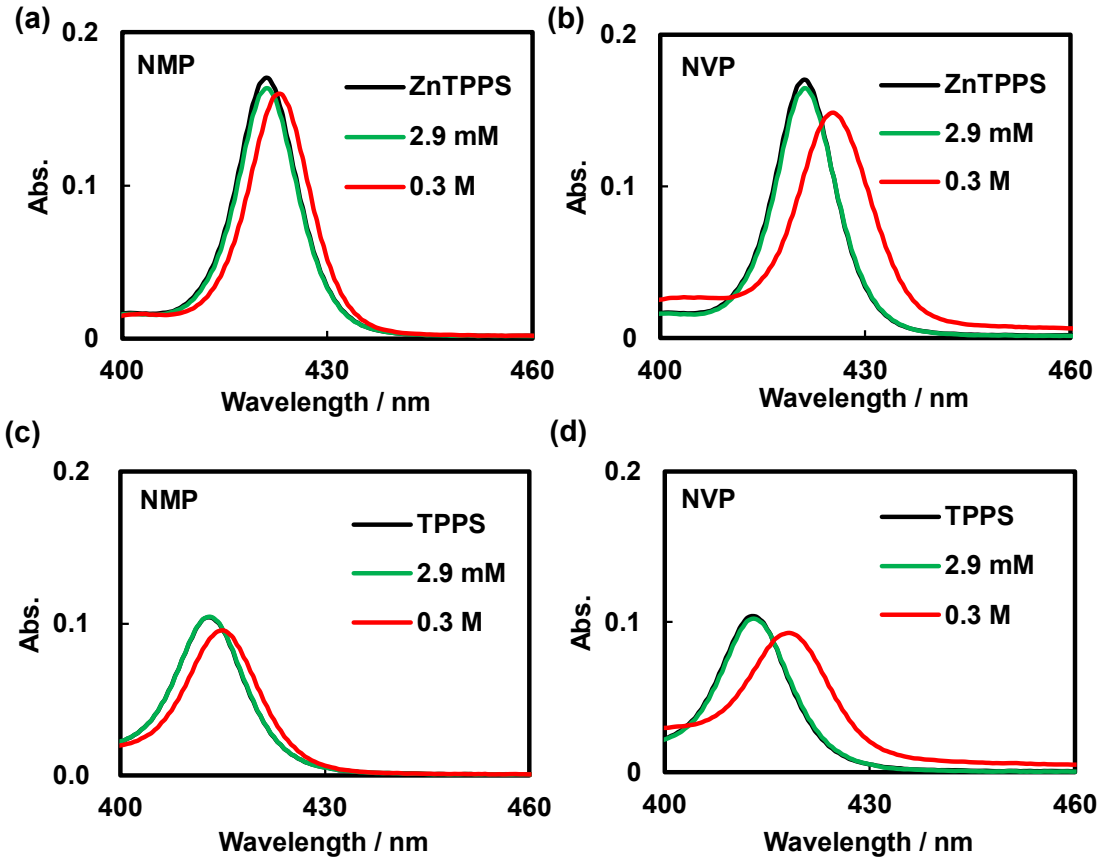

Fig. 2-10. Absorption spectra of (a) ZnTPPS and (b) TPPS upon the addition of NMP; Absorption spectra of (c) ZnTPPS and (d) TPPS up on the addition of NVP.

Additionally, studying the interaction between ZnTPPS and PVP with different

molecular weights (PVP 25 (M = 24,500), PVP K-90 (M = 360,000)) revealed no discernible molecular weight dependence (Fig. 2-11). Despite testing, polyethylene glycol (PEG) failed to form a complex with ZnTPPS (Fig. 2-11).

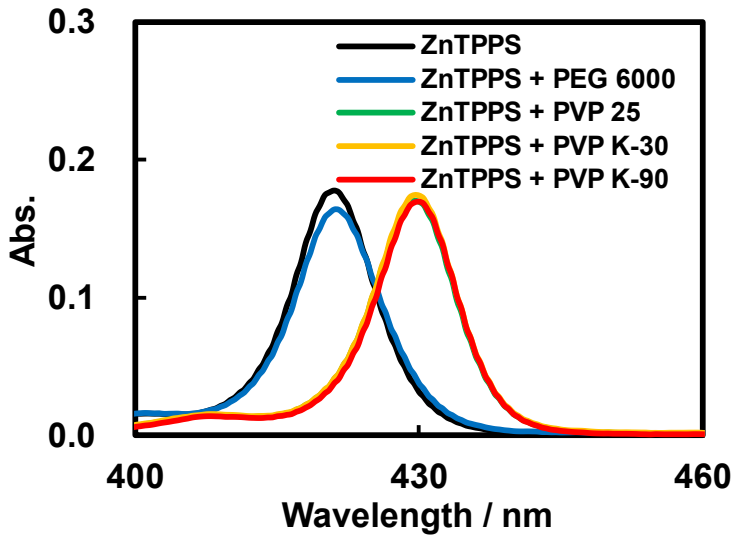

Fig. 2-11. Absorption spectra of ZnTPPS upon the addition of PEG or PVP.

2-3.2. Photoinduced Electron Transfer

In the presence of MV^{2+}, both ZnTPPS and TPPS form donor–acceptor pairs with MV^{2+}.[34] Addition of MV^{2+} to TPPS or ZnTPPS led to observable redshifts in their absorption spectra (Figs. 2-12a and 2-12b). However, upon the addition of MV^{2+} in the presence of PVP in the TPPS or ZnTPPS solution, no significant peak shifts were observed (Figs. 2-12c and 2-12d). These results imply a restrained ground-state interaction between the porphyrin and MV^{2+} in the presence of PVP.

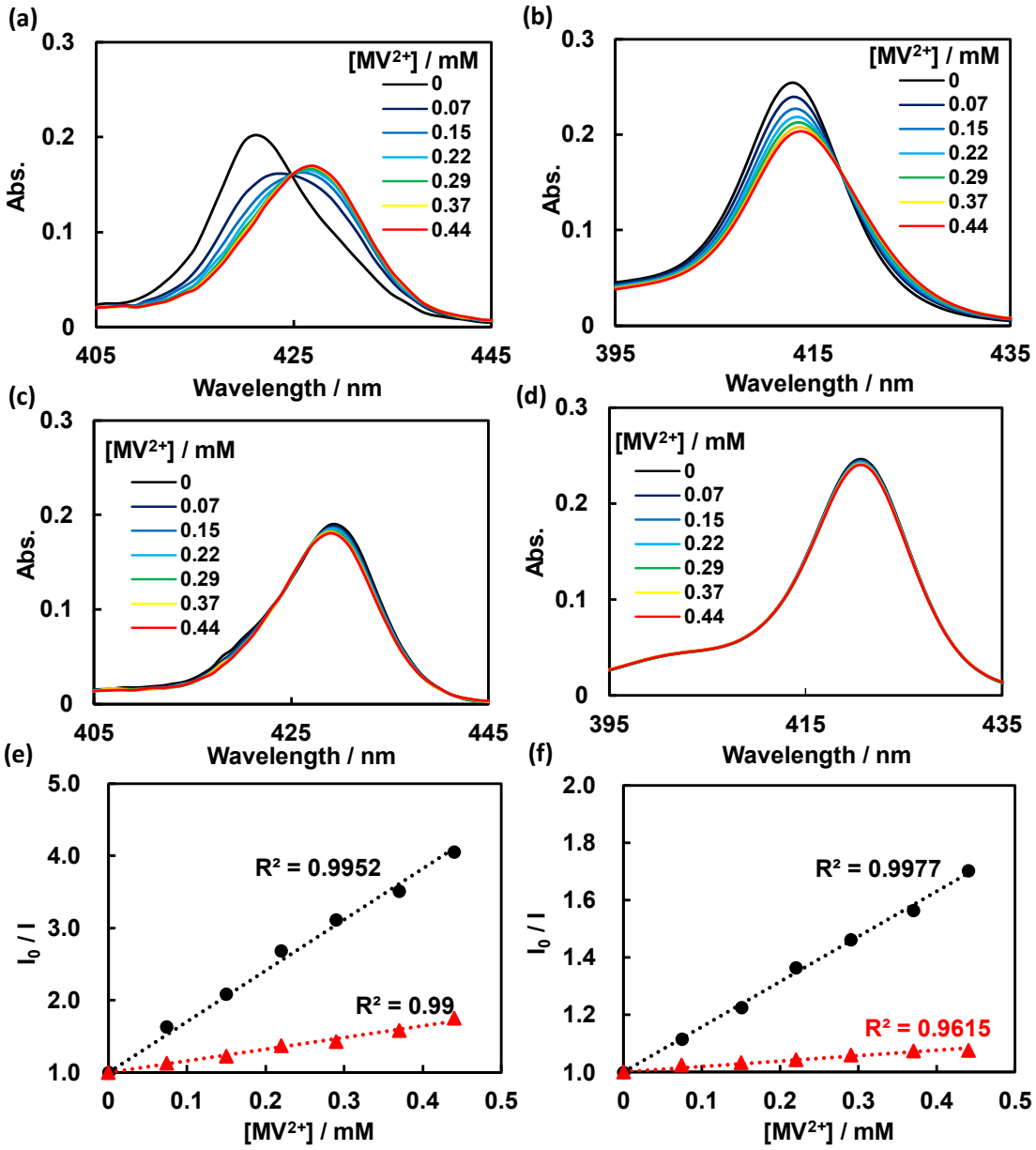

Fig. 2-12. Absorption spectra of (a) ZnTPPS and (b) TPPS upon the addition of MV^{2+}; Absorption spectra of (c) ZnTPPS and (d) TPPS upon the addition of MV^{2+} with 24.0 μM PVP existence; Stern–Volmer plots of the quenching of (e) ZnTPPS and (f) TPPS by MV^{2+} in the absence (solid circles) and presence (solid triangles) of 24.0 μM PVP.

Further investigation involved observing the fluorescence quenching of ZnTPPS (Fig. 2-13) and TPPS (Fig. 2-14) by MV^{2+} with and without 24.0 μM PVP upon excitation at

the isosbestic point, aiming to understand the electron transfer from the porphyrins to MV^{2+}. Stern–Volmer (SV) plots constructed based on the intensity at the maximum of fluorescence band (Figs. 2-12e and 2-12f) revealed a decrease in the SV constant (K_{SV}) upon the addition of PVP ($K_{SV,\ ZnTPPS–MV}$: 7.1 to 1.6, $K_{SV,\ TPPS–MV}$: 1.6 to 0.2), indicating a reduced fluorescence quenching efficiency. However, notable fluorescence quenching was still observed.

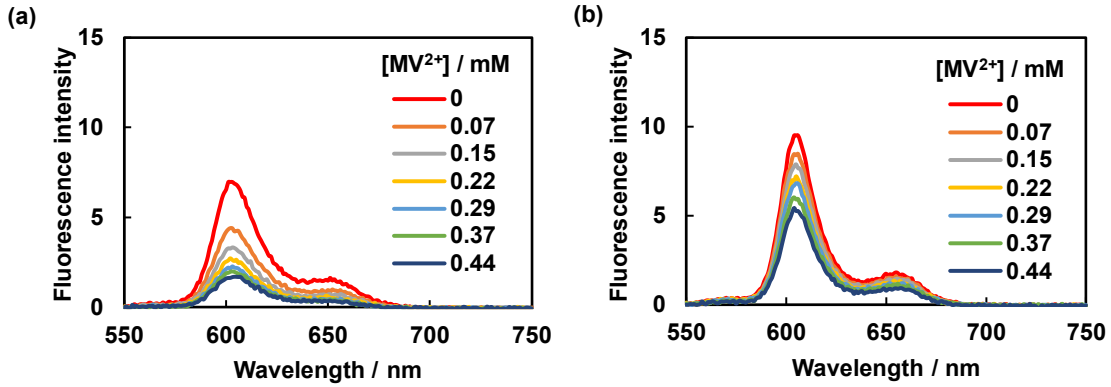

Fig. 2-13. Fluorescence spectra 0.6 μM ZnTPPS upon the addition of MV^{2+} in the (a) absence and (b) presence of 24.0 μM PVP.

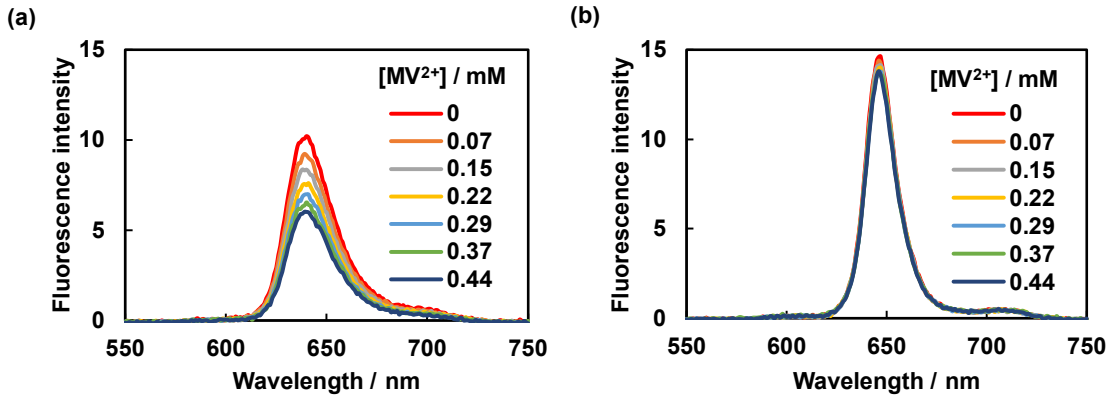

Fig. 2-14. Fluorescence spectra 0.6 μM TPPS upon the addition of MV^{2+} in the (a) absence and (b) presence of 24.0 μM PVP.

The absence of spectral overlap between the emission spectra of porphyrin and the absorption spectra of MV^{2+} indicates the absence of Förster energy transfer. The fluorescence quenching experiments were conducted in the presence of oxygen, which typically depletes the triplet state of porphyrin. Moreover, the direct interaction between MV^{2+} and porphyrins was hindered by PVP, making molecular collisions less likely to occur. This effect was consistent with the similar fluorescence quenching behavior observed in the presence and absence of oxygen (Figs. 2-13b and 2-15a). Thus, the decline in fluorescence intensity can be attributed to photoinduced electron transfer occurring over long distances.

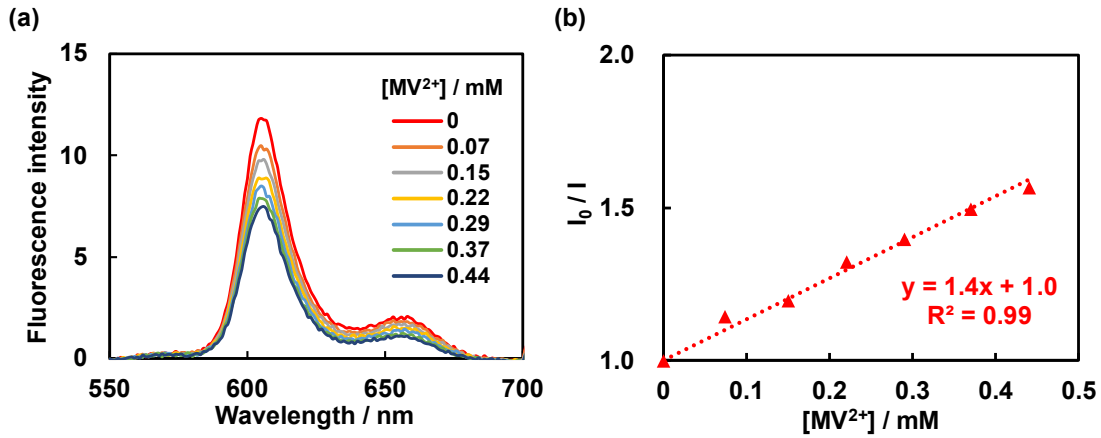

Fig. 2-15. (a) Fluorescence spectra of ZnTPPS upon the addition of MV^{2+} in the absence of oxygen; (b) Stern–Volmer plots of the quenching of ZnTPPS by MV^{2+} in absence of oxygen.

PVP 25 and K-90 (0.24 mM) demonstrated similar abilities in regulating the interaction and photoinduced electron transfer between ZnTPPS and MV^{2+}, with no observable

dependence on molecular weight (Figs. 2-16–2-18). Conversely, PEG (0.24 mM) did not exhibit any control over the interaction or the photoinduced electron transfer between ZnTPPS and MV^{2+} (Figs. 2-16–2-18).

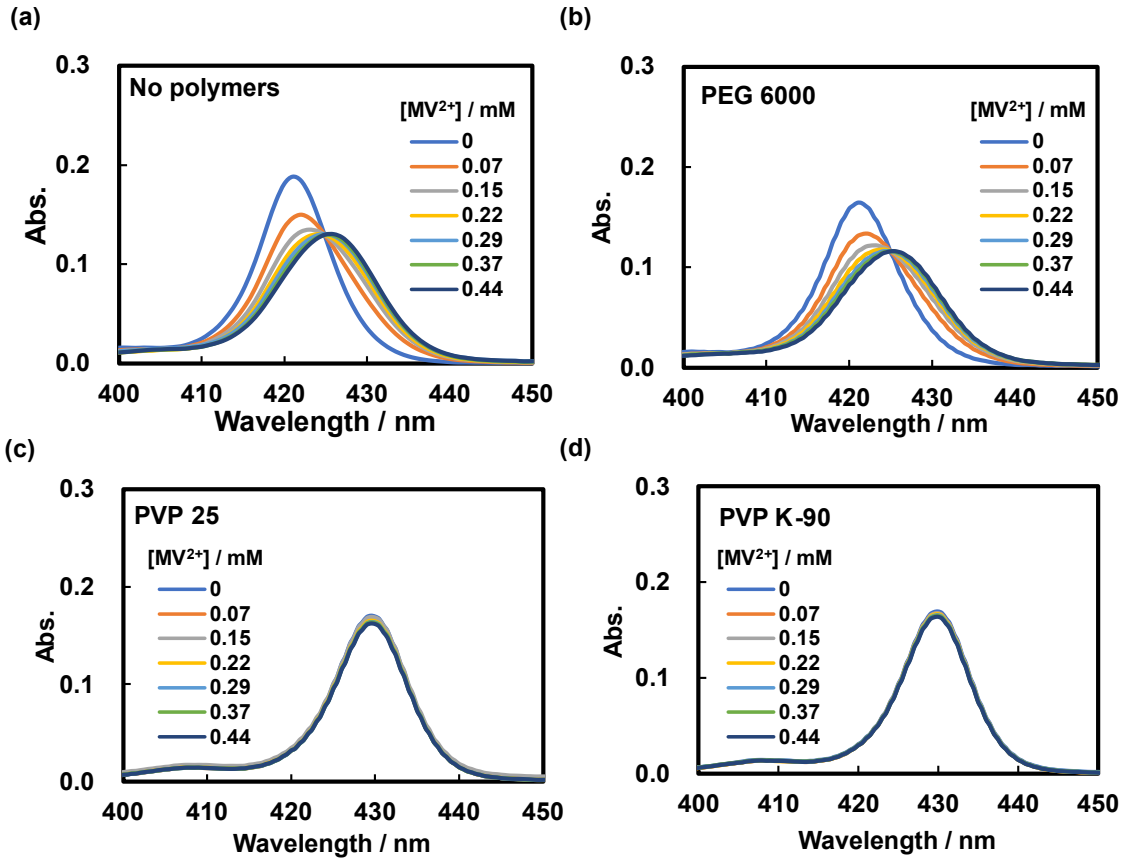

Fig. 2-16. Absorption spectra of ZnTPPS upon the addition of MV^{2+} in the (a) absence and presence of 0.24 mM (b) PEG, (c) PVP 25 and (d) PVP K-90.

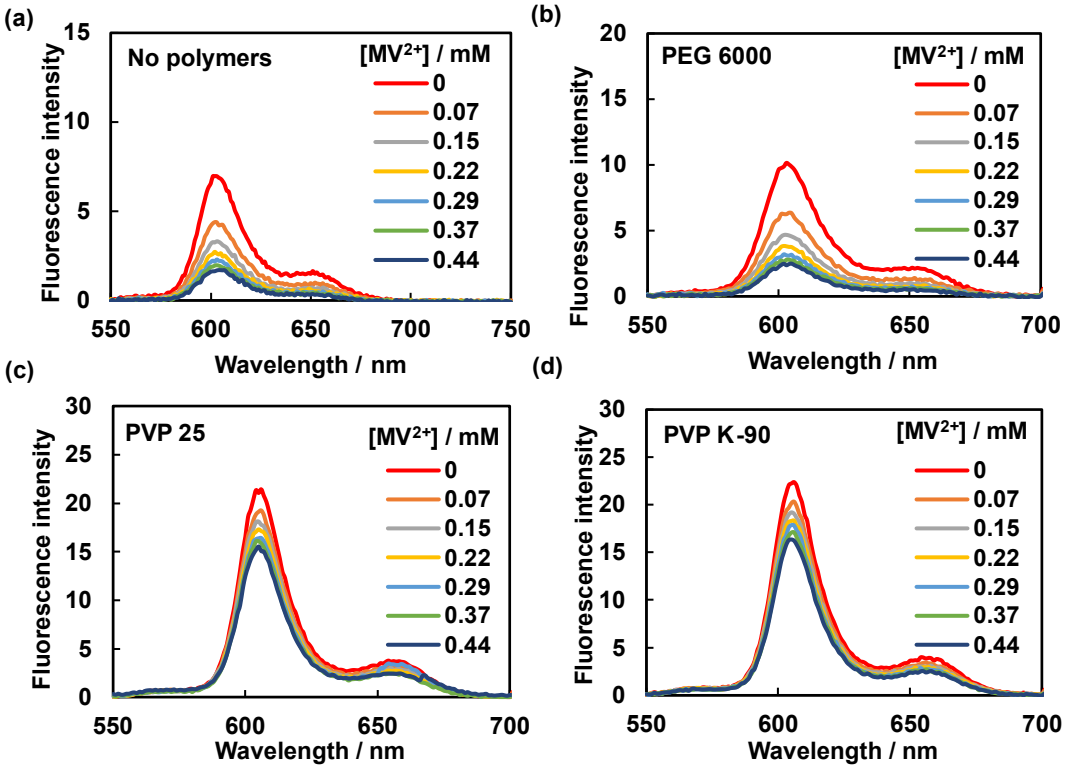

Fig. 2-17. Fluorescence spectra of ZnTPPS upon the addition of MV^{2+} in the (a) absence and presence of 0.24 mM (b) PEG, (c) PVP 25 and (d) PVP K-90.

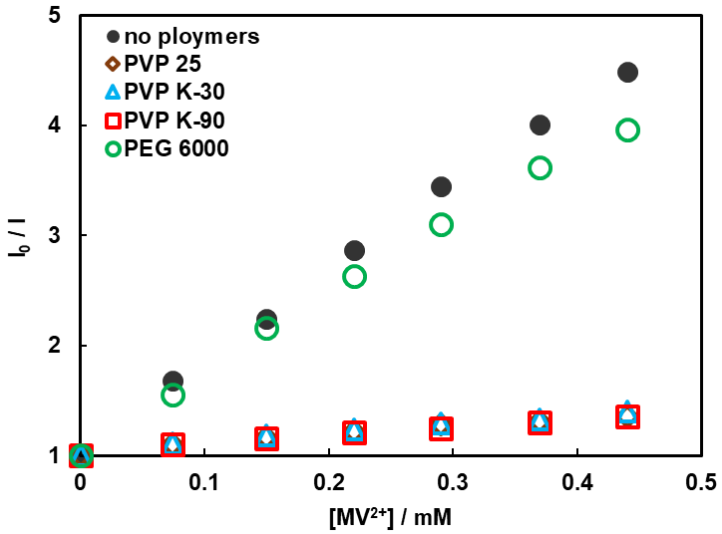

Fig. 2-18. Stern–Volmer plots for the quenching of ZnTPPS by MV^{2+} in the absence and presence of PEG or PVP.

The higher quantum yield of ZnTPPS compared to TPPS and its elevated energy level facilitate electron transfer from ZnTPPS to MV^{2+} more readily than that from TPPS.[35,36] Therefore, ZnTPPS was selected for subsequent experiments. Ethylenediamine-*N*,*N*,*N*′,*N*′-tetraacetic acid tetrasodium salt (EDTA) was introduced as a sacrificial agent to enable the reduction of oxidized ZnTPPS after the photoinduced electron transfer process (Scheme 2-1).

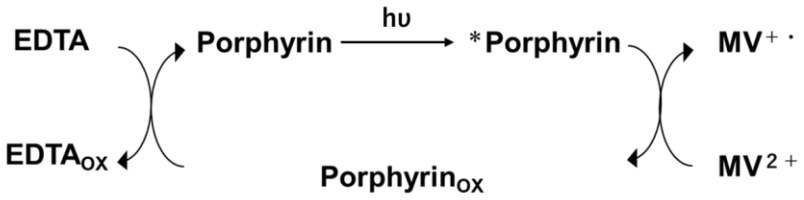

Scheme 2-1. Generation of $MV^{+\bullet}$ from MV^{2+} via electron transfer from photoexcited porphyrin with EDTA as a sacrificial agent.

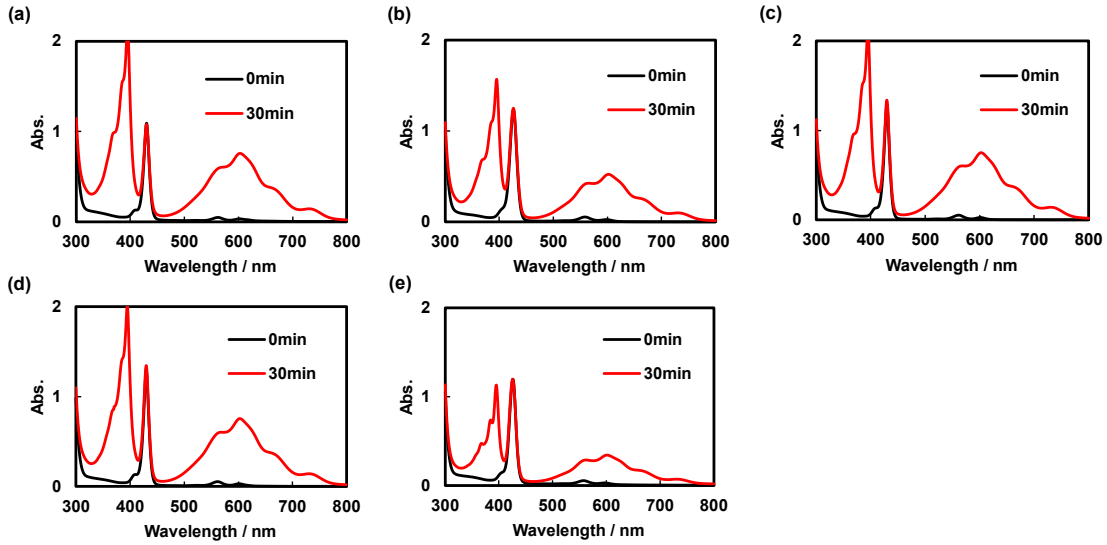

Fig. 2-19. Absorption spectra of mixed solutions of ZnTPPS, MV^{2+}, and EDTA in the (a) absence and (b–e) presence of PVP at various ratios: (b) 4 eq., (c) 40 eq., (d) 400 eq. and (e) 4000 eq. before and after 30 min of irradiation.

Degassed solutions of ZnTPPS, PVP, MV^{2+}, and EDTA as a sacrificial agent were irradiated with UV light at ~20 cm for 30 minutes, causing a change in the absorbance at 605 nm (ΔAbs), indicating the presence of the methylviologen cationic radical ($MV^{+\bullet}$) (Fig. 2-19).[37]

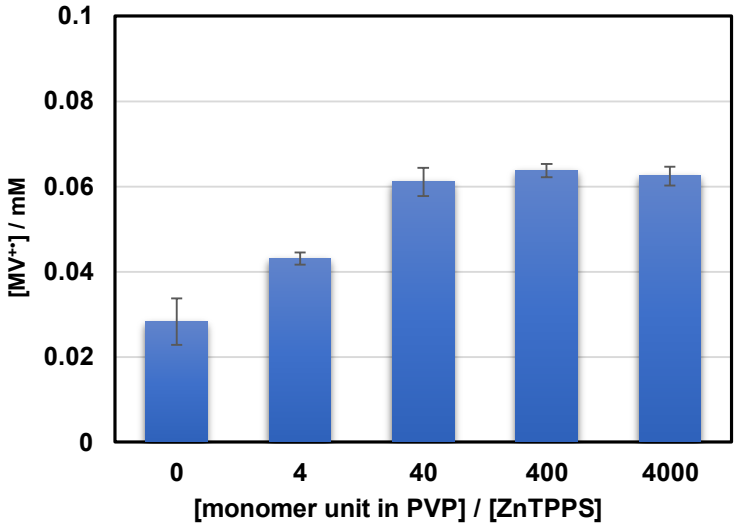

Fig. 2-20. Generated $MV^{+\bullet}$ in ZnTPPS systems, in the absence and presence of PVP.

The concentrations of generated $MV^{+\bullet}$ were determined by monitoring the change in absorbance at 605 nm, in conjunction with its molar absorption coefficient.[37] Concentration of the generated $MV^{+\bullet}$ increased with increasing the PVP concentration (Fig. 2-20) and reached saturation at higher PVP concentrations. Despite the diminished electron transfer environment between ZnTPPS and MV^{2+} following the addition of PVP (as indicated by the significantly lower K_{SV} value), the concentration of generated $MV^{+\bullet}$ reached a peak value of ~0.06 mM. This outcome suggests the critical role of PVP in impeding reverse electron transfer within this photoinduced electron-transfer process.[24,26]

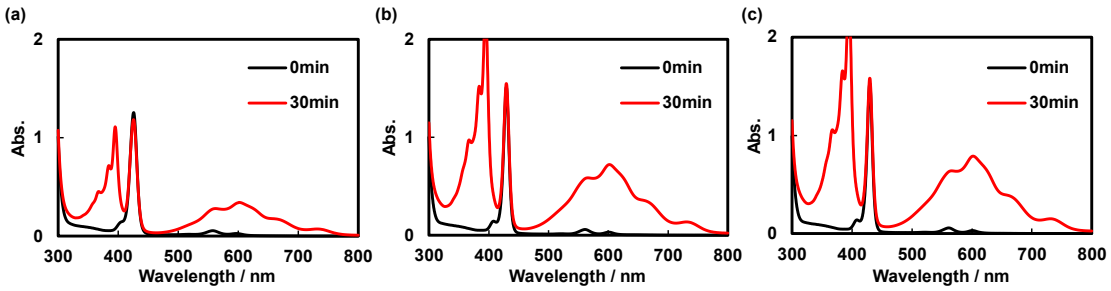

Fig. 2-21. Absorption spectra of mixed solutions of ZnTPPS, MV^{2+}, and EDTA in the presence of 0.24 mM (a) PEG, (b) PVP 25 or (c) PVP K-90 before and after 30 min of irradiation under UV light.

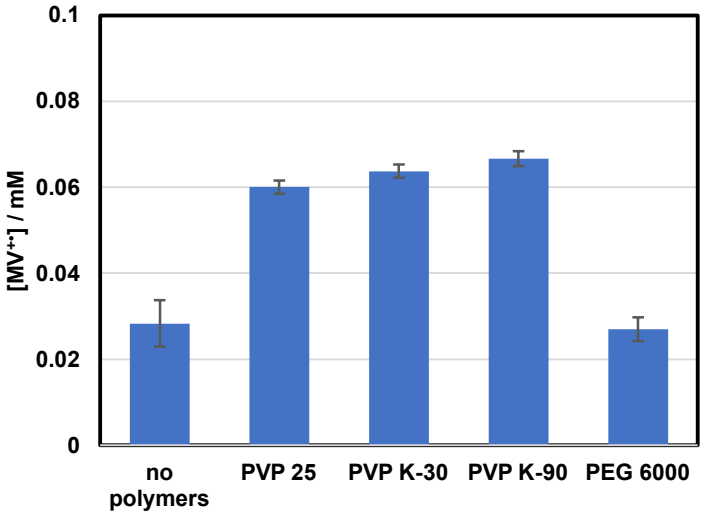

Fig. 2-22. Generated $MV^{+\bullet}$ in ZnTPPS systems, in the absence and presence of 0.24 mM PVP or PEG.

PVP 25 and K-90 similarly contributed to the production of $MV^{+\bullet}$ (Figs. 2-21 and 2-22), with minimal dependence on their respective molecular weights. Conversely, PEG exhibited no discernible impact on the production of $MV^{+\bullet}$ (Figs. 2-21 and 2-22).

2-4. Conclusions

In this study, PVP demonstrated its ability to form complexes with ZnTPPS and TPPS through coordination bonding with ZnTPPS and hydrogen bonding with TPPS. These complex formations effectively regulated the interactions between the ground-state porphyrins and MV^{2+} while also influencing the photoinduced electron transfer from porphyrins to MV^{2+}. The presence of PVP notably increased the production of an electron transfer product ($MV^{+\bullet}$) via photoinduced electron transfer from ZnTPPS to MV^{2+}. Our ongoing investigations aim to explore the conversion of the generated $MV^{+\bullet}$ into storable energy forms, such as hydrogen or formic acid,[27,38] thereby realizing the conversion of solar energy into chemical energy.

This study presents a versatile and convenient approach to control photoinduced electron transfer between diverse electron donor and acceptor pairs. Leveraging appropriate polymers, this method exhibits promising adaptability across a spectrum of donor-acceptor combinations.

References

1. Zhang, Q.; Suresh, L.; Liang, Q.; Zhang, Y.; Yang, L.; Paul, N.; Tan, S. *Adv. Sustain. Syst.* **2021**, *5*, 19.
2. Hussain, S.; Ulhassan, Z.; Brestic, M.; Zivcak, M.; Zhou, W.; Allakhverdiev, S.; Yang, X.; Safdar, M.; Yang, W.; Liu, W. *Photosyn. Res.* **2021**, *150*, 5–19.
3. Li, X.; Zhao, L.; Yu, J.; Liu, X.; Zhang, X.; Liu, H.; Zhou, W. *Nanomicro Lett.* **2020**, *12*, 29.
4. Deisenhofer, J.; Michel, H. *Biosci. Rep.* **2004**, *24*, 323–361.
5. McConnell, I.; Li, G.; Brudvig, G. *Chem. Biol.* **2010**, *17*, 434–447.
6. Wang, Y.; Suzuki, H.; Xie, J.; Tomita, O.; Martin, D.; Higashi, M.; Kong, D.; Abe, R.; Tang, J. *Chem. Rev.* **2018**, *118*, 5201–5241.
7. Zhang, B.; Sun, L. *Chem. Soc. Rev.* **2019**, *48*, 2216–2264.
8. Fang, X.; Kalathil, S.; Reisner, E. *Chem. Soc. Rev.* **2020**, *49*, 4926–4952.
9. Pannwitz, A.; Klein, D.; Rodriguez-Jimenez, S.; Casadevall, C.; Song, H.; Reisner, E.; Hammarstrom, L.; Bonnet, S. *Chem. Soc. Rev.* **2021**, *50*, 4833–4855.
10. Gust, D.; Moore T.; Moore A. *Acc. Chem. Res.* **2009**, *42*, 1890–1898.
11. Fukuzumi, S.; Ohkubo, K.; Suenobu, T. *Acc. Chem. Res.* **2014**, *47*, 1455–1464.
12. Urbani, M.; Gratzel, M.; Nazeeruddin M.; Torres, T. *Chem. Rev.* **2014**, *114*, 12330–12396.
13. Fukuzumi, S.; Lee, Y.; Nam, W. *Tetrahedron* **2020**, *76*, 131024.
14. Pachfule, P.; Acharjya, A.; Roeser, J.; Sivasankaran, R.; Ye, M.; Bruckner, A.; Schmidt, J.; Thomas, A. *Chem. Sci.* **2019**, *10*, 8316–8322.
15. Zhu, Y.; Zhu, D.; Chen, Y.; Yan, Q.; Liu, C.; Ling, K.; Liu, Y.; Lee, D.; Wu, X.; Senftle, T.; Verduzco, R. *Chem. Sci.* **2021**, *12*, 16092–16099.

16. Aoyama, Y.; Asakawa, M.; Matsui, Y.; Ogoshi, H. *J. Am. Chem. Soc.* **1991**, *113*, 6233–6240.
17. Sessler, J.; Sathiosatham, M.; Brown, C.; Rhodes T.; Wiederrecht, G. *J. Am. Chem. Soc.* **2001**, *123*, 3655–3660.
18. Bottari, G.; de la Torre, G.; Guldi, D.; Torres, T. *Chem. Rev.* **2010**, *110*, 6768–6816.
19. Otsuki, J. *J. Mater. Chem. A.* **2018**, *6*, 6710–6753.
20. Zarrabi, N.; Poddutoori, P. *Coord. Chem. Rev.* **2021**, *429*, 213561.
21. Sadamoto, R.; Tomioka, N.; Aida, T. *J. Am. Chem. Soc.* **1996**, *118*, 3978–3979.
22. Wang, X.; Zhao, L.; Ma, R.; An Y.; Shi, L. *Chem. Commun.* **2010**, *46*, 6560–6562.
23. Wang, R.; Qu, R.; Jing, C.; Zhai, Y.; An Y.; Shi, L. *RSC Adv.* **2017**, *7*, 10100–10107.
24. Harada, A.; Yamaguchi, H.; Okamoto, K.; Fukushima, H.; Shiotsuki, K.; Kamachi, M. *Photochem. Photobiol*. **1999**, *70*, 298–302.
25. Yamaguchi, H.; Kamachi M.; Harada, A. *Angew. Chem. Int. Ed.* **2000**, *39*, 3829–3831.
26. Onji, T.; Ohara, H.; Yamaguchi, H.; Ikeda, N.; Harada, A. *Chem. Lett.* **2006**, *35*, 1126–1127.
27. Yamaguchi, H.; Onji, T.; Ohara, H.; Ikeda, N.; Harada, A. *Bull. Chem. Soc. Jpn.* **2009**, *82*, 1341–1346.
28. Flamigni, L.; Talarico, A.; Ventura, B.; Rein, R.; Solladie, N. *Chem. Eur. J.* **2006**, *12*, 701–712.
29. Huo, D.; Yang, L.; Hou, C.; Fa, H.; Luo, X.; Lu, Y.; Zheng, X.; Yang, J.; Yang, L. *Spectrochim. Acta A Mol. Biomol. Spectrosc.* **2009**, *74*, 336–343.
30. Nappa, M.; Valentine, J. *J. Am. Chem. Soc.* **1978**, *100*, 5075–5080.
31. Lin, C.; Fang M.; Cheng, S. *J. Electroanal. Chem.* **2002**, *531*, 155–162.
32. Soury, R.; Jabli, M.; Saleh, T.; Abdul-Hassan, W.; Saint-Aman, E.; Loiseau, F.;

Philouze, C.; Nasri, H. *RSC Adv.* **2018**, *8*, 20143–20156.

33. Maiti, N.; Mazumdar, S.; Periasamy, N. *J. Phys. Chem. B* **1998**, *102*, 1528–1538.
34. Logunov, S.; Rodgers, M. *J. Photochem. Photobiol. A* **1997**, *105*, 55–63.
35. Kalyanasundaram, K. *J. Chem. Soc. Faraday Trans. 2* **1983**, *79*, 1365–1374.
36. Osuka, A.; Shin, J.; Yoneshima, R.; Shiratori, H.; Ohno, T.; Nozaki, K.; Nishimura, Y.; Yamazaki, I.; Taniguchi, S.; Shimizu, T.; Okada, T. *J. Porphyr. Phthalocyanines* **1999**, *3*, 729–741.
37. Watanabe, T.; Honda, K. *J. Phys. Chem.* **1982**, *86*, 2617–2619.
38. Ikeyama, S.; Amao, Y. *Sustain. Energy Fuels* **2017**, *1*, 1730–1733.

Chapter 3

Controlled Photoinduced Electron Transfer via Triplet in Polymer Matrix Using Electrostatic Interactions

3-1. Introduction

In recent years, the study of electron transfer processes within complex molecular systems has garnered increasing attention due to its pivotal role in a wide range of scientific and technological applications.[1–4] Among the diverse array of molecular systems, porphyrins have emerged as fascinating candidates for exploring electron transfer dynamics. These aromatic macrocycles exhibit unique photophysical properties, making them ideal platforms for investigating charge transfer and energy transfer phenomena .[5,6]

In particular, the interaction between porphyrins and various electron acceptors within a polymer matrix has captured the interest of researchers seeking to understand and control these processes.[7–12] These systems' potential applications span diverse fields, including photovoltaics,[13–15] sensors,[16,17] and molecular electronics.[18,19]

This study delves into the intricate electron transfer dynamics within systems consisting of porphyrin (TPPS and ZnTPPS), polymer (poly(*N*-methyl-4-vinylpyridinium), P4VPMe), and electron acceptor (MV^{2+}), with a focus on the role of the polymer matrix in modulating these interactions (Fig. 3-1).

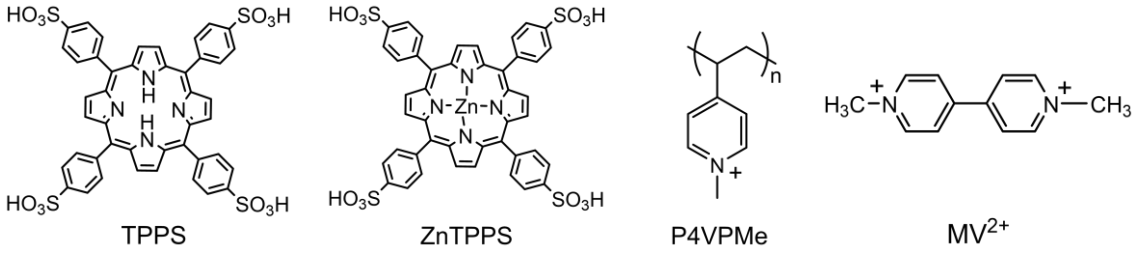

Fig. 3-1. Chemical structures of TPPS, ZnTPPS, P4VPMe and MV^{2+}.

3-2. Experimental Section

Materials

5,10,15,20-Tetrakis-(4-sulfonatophenyl) porphyrin (TPPS) was purchased from TCI Co., Ltd., Tokyo, Japan. Methyl viologen hydrate, potassium dihydrogenphosphate, dipotassium hydrogenphosphate, ethylenediamine-*N*,*N*,*N*′,*N*′-tetraacetic acid tetrasodium salt (EDTA), 4-vinyl pyridine and 2,2' azobis(2-vmethylpropionitrile) (AIBN) were purchased from Nacalai Tesque, Kyoto, Japan. All the reagents and solvents, except 4-vinyl pyridine, were used as received without further purification. 4-Vinyl pyridine was distillated to remove the polymerization inhibitor (hydroquinone) within it before polymerization. Zinc *meso*-5,10,15,20-tetrakis-(4-sulfonatophenyl)porphyrin (ZnTPPS) was prepared according to the method reported by Flamigni et al.[20] Poly (4-vinyl pyridine) was prepared by polymerize 4-vinyl pyridine in DMF using AIBN as a thermal initiator. Poly(*N*-methyl-4-vinylpyridinium) (P4VPMe) was synthesized by methylating poly 4-vinyl pyridine in methanol using iodomethane.

Methods

^{1}H NMR spectra were acquired with a JEOL JNM-ECA 500 MHz NMR spectrometer (Tokyo, Japan). The chemical shifts were referenced to the solvent value (δ = 4.79 ppm for D_2O). Gel permeation chromatography (GPC) was performed at 25 °C on a TOSOH HLC-8320GPC EcoSEC® system equipped with an RI detector and TOSOH TSK gel α-M column, using dimethyl sulfoxide (DMSO) containing lithium bromide (1.05 g L^{-1}) as the eluent at a flow rate of 0.4 mL min^{-1}. The molecular weights were calibrated with seven standard samples of poly(ethylene glycol) (PEG) (Scientific Polymer Products, Inc. (Ontario, NY)). Sample solutions were filtrated with a DISMIC13JP PTFE 0.50 μm filter just prior to injection. UV-visible spectra were recorded using a SHIMADZU UV-2500PC spectrophotometer (Kyoto, Japan) at 25 °C. A quartz cuvette with an optical path length of 1 cm was used for these measurements. Excitation and fluorescence spectra were obtained with a HITACHI F-2500 fluorescence spectrophotometer (Tokyo, Japan) at 25 °C, employing 1-cm quartz cuvettes. Slit widths were both 5.0 nm for excitation and emission side and sensitivity was set to high. Irradiation experiments were conducted in a sealed 1-cm quartz cuvette using an USHIO SP-11 UV irradiation unit with a HOYA ND10 filter. Emission lifetimes were measured with a home-built setup based on the time-correlated single-photon counting. The details were described in a previous report.[21] The pulsed light source was a Ti:sapphire oscillator, and the second harmonics at 420 nm was used for photoexcitation of the sample. The instrumental response function was evaluated as 48 ps. Transient absorption spectra in the nanosecond and microsecond time regions were measured using a home-built setup.[22] The excitation light source was a Nd:YAG laser and the second harmonics at 532 nm was used for photoexcitation of the sample.

The time resolution of the measurement was ca. 50 ns. In the transient absorption measurements, the sample solution was filled into a 1 cm cuvette and deoxygenated with nitrogen bubbling in 10 minutes unless specifically mentioned.

Synthesis

Synthesis of P4VP and P4VPMe

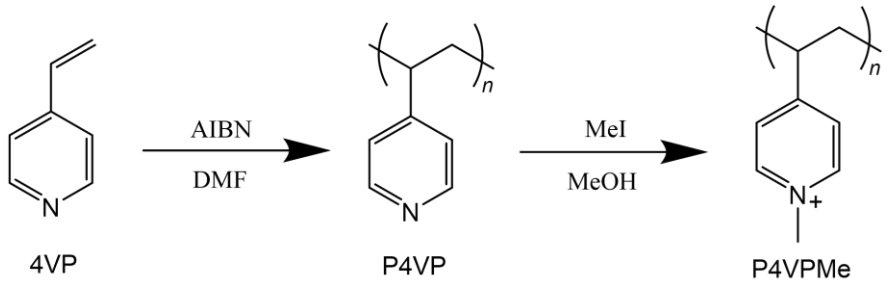

Scheme 3-1. Synthesis of P4VPMe.

Poly(4-vinylpyridine) (P4VP) was prepared by polymerizing 4-vinylpyridine in DMF using AIBN as a thermal initiator (Scheme 3-1). Initially, 1.0 g (10.0 mmol) of distilled 4-vinylpyridine was dissolved in 10 mL of DMF. Varying amounts (0.1 mmol and 0.2 mmol) of AIBN were subsequently added, and the mixture was refluxed at 60 °C for 24 h. Following this, the solution was poured into 100 mL of diethyl ether, and the resulting particulate (P4VP) was collected after being washed three times with diethyl ether. GPC measurements (Fig. 3-2) revealed molecular weights (M_n) of 3,700 and 6,400, respectively.

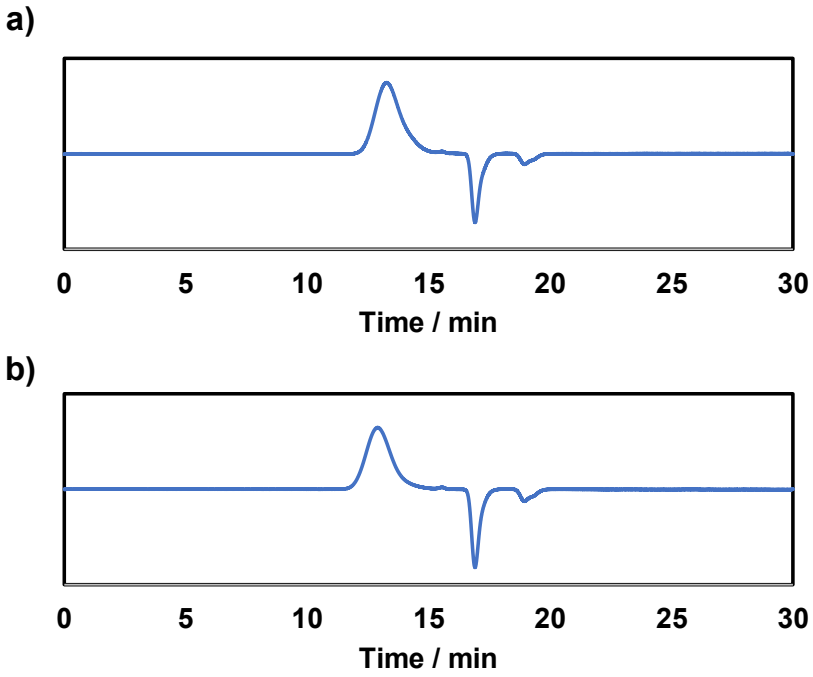

Fig. 3-2. GPC profiles of P4VP with molecular weights of 3,700 and 6,400.

P4VPMe was prepared by quaternization of poly(4-vinylpyridine) in methanol using iodomethane (Scheme 3-1). Initially, 0.1 g (1.0 mmol) of P4VP was dissolved in 5.0 mL of methanol. Then, 0.6 mL (10.0 mmol) of iodomethane was added, and the mixture was stirred at room temperature for 40 h. Subsequently, the resulting particulate (P4VPMe) was collected by centrifugation and washed three times with methanol. Quantitative methylation was confirmed by ^{1}H NMR analysis (Fig. 3-3). The molecular weights (M_n) of P4VPMe were calculated to be 4,300 and 7,400.

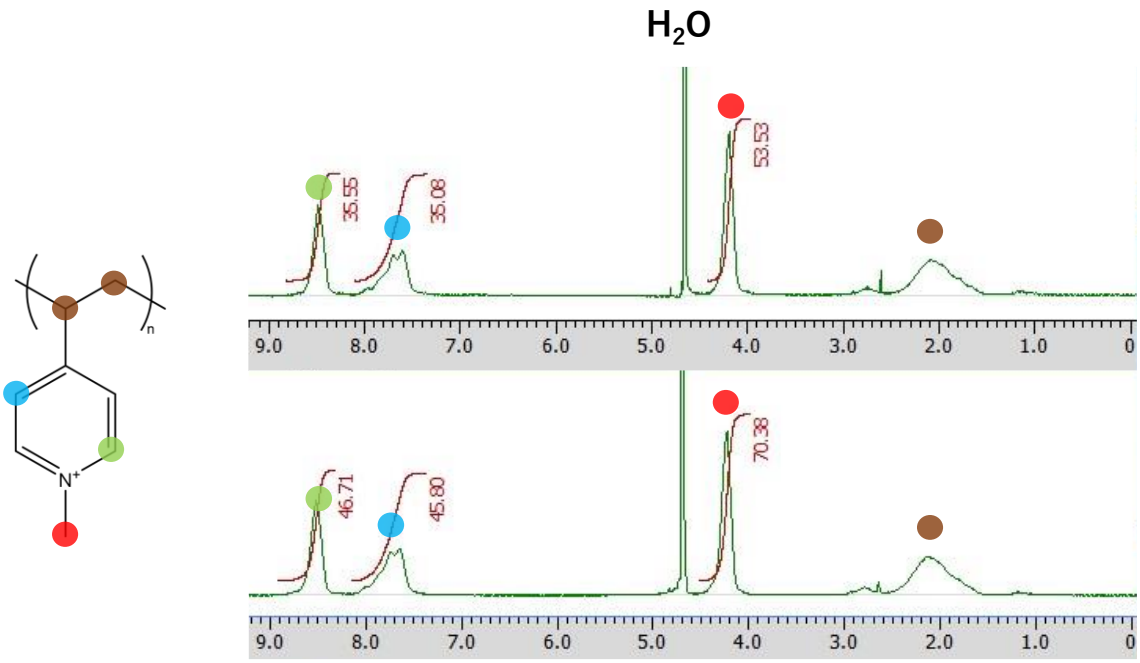

Fig. 3-3. ^{1}H NMR spectra of P4VPMe with molecular weights of 4,300 and 7,400.

3-3. Result and Discussion

3-3.1. Evolution of Porphyrin Aggregates in P4VPMe Polymer Matrix

To investigate the interaction of ZnTPPS with P4VPMe, absorption spectra of mixed solutions of ZnTPPS and P4VPMe (M_n = 4,300) at different charge ratios (I = c_{charge}(prophryin) / c_{charge}(P4VPMe)) in a 0.01 M phosphate buffer (pH = 8.0) were recorded. The Soret band of ZnTPPS, with a maximum absorption at 420 nm, exhibited a redshift upon the addition of P4VPMe (I = 0.10) and broadened into a multi-component band, displaying peaks at 410, 430 and 440 nm simultaneously (Fig. 3-4a). Further addition of P4VPMe led to an increase in absorbance at 430 nm and a decrease in absorbance at 410 and 440 nm. Ultimately, in the presence of an excess of P4VPMe (I = 0.01), a single-component band at 430 nm was observed.

Excitation spectra (λ_{em} = 605 nm) of these mixed solutions were recorded to identify the components that appeared upon the addition of P4VPMe. When ZnTPPS was irradiated at 420 nm, it emitted at 605 nm when in isolation. However, in the presence of P4VPMe, ZnTPPS emitted light only when irradiated at 430 nm, regardless of the quantity of P4VPMe added (Fig. 3-4b). Therefore, the 430 nm absorption band was assignable to a single molecule of ZnTPPS within the P4VPMe polymer matrix, while the absorption bands at 410 and 440 nm were ascribed to be (J or H) aggregates of ZnTPPS within the P4VPMe polymer matrix.[23,24]

It can be concluded that, as the addition of P4VPMe progressed, ZnTPPS initially formed aggregates at low P4VPMe concentrations. Subsequently, these aggregates gradually dissociated into individual ZnTPPS molecules as the P4VPMe reached an excess amount (Fig. 3-7a), as illustrated in the spectral data and discussed in Figs. 3-4a and 3-4b. Furthermore, the aggregation and dissociation of ZnTPPS in the P4VPMe polymer matrix were also examined and supported by excited singlet lifetime measurements of ZnTPPS with P4VPMe (upon the addition of P4VPMe, the singlet lifetime of ZnTPPS initially decreased and then recovered in the presence of an excess of P4VPMe; see Table 3-1).

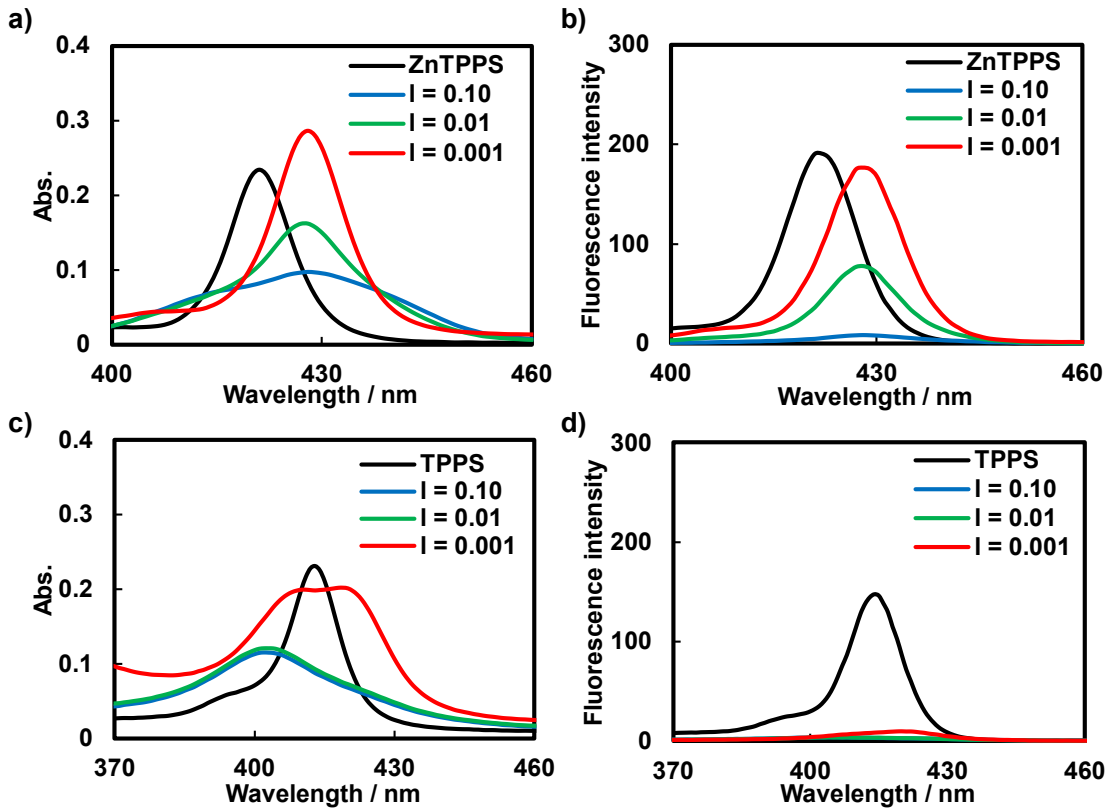

Fig. 3-4. Absorption spectra of mixing solutions of P4VPMe and a) ZnTPPS or c) TPPS at various charge ratios. Excitation spectra of mixing solutions of P4VPMe and b) ZnTPPS or d) TPPS at various charge ratios.

Absorption spectra and excitation spectra (λ_{em} = 640 nm) of mixed solutions of TPPS and P4VPMe at different *I* in a 0.01M phosphate buffer (pH = 8.0) were also recorded. Notable changes, such as shifting and broadening, were observed in the Soret band of TPPS upon the addition of P4VPMe (Fig. 3-4c). However, none of these changes resulted in obvious emission (Fig. 3-4d). This suggests that TPPS forms aggregates when mixed with P4VPMe, and these aggregates persist even in the presence of an excess of P4VPMe (Fig. 3-7b). The aggregation of TPPS in the P4VPMe polymer matrix was further confirmed through excited singlet lifetime measurements. With the addition of P4VPMe,

the lifetime of TPPS consistently decreased in one direction (Table 3-1), providing additional evidence for the formation of TPPS aggregates within the P4VPMe polymer matrix.

Excited singlet-state lifetime measurements of ZnTPPS and TPPS (0.6 μM) in the absence and presence of P4VPMe (M_n = 4,300) at varying charge ratios (0.10, 0.01 and 0.001) in 0.01 M phosphate buffer (pH 8.0) were carried out. The associated data are presented in Figs. 3-5 and 3-6.

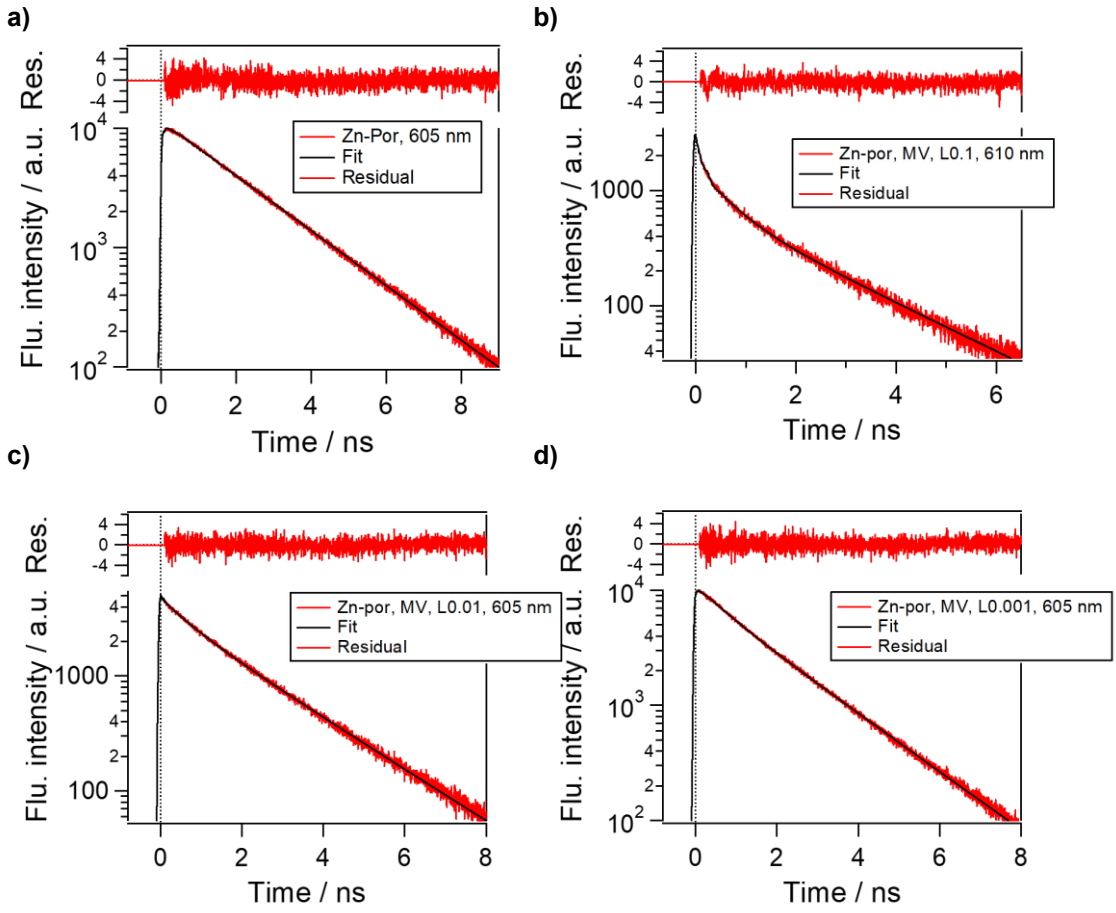

Fig. 3-5. Fluorescence decay profiles of ZnTPPS in the a) absence of P4VPMe and presence of P4VPMe (M_n = 4,300) at varying charge ratios: b) I = 0.10, c) I = 0.01 and d) I = 0.001.

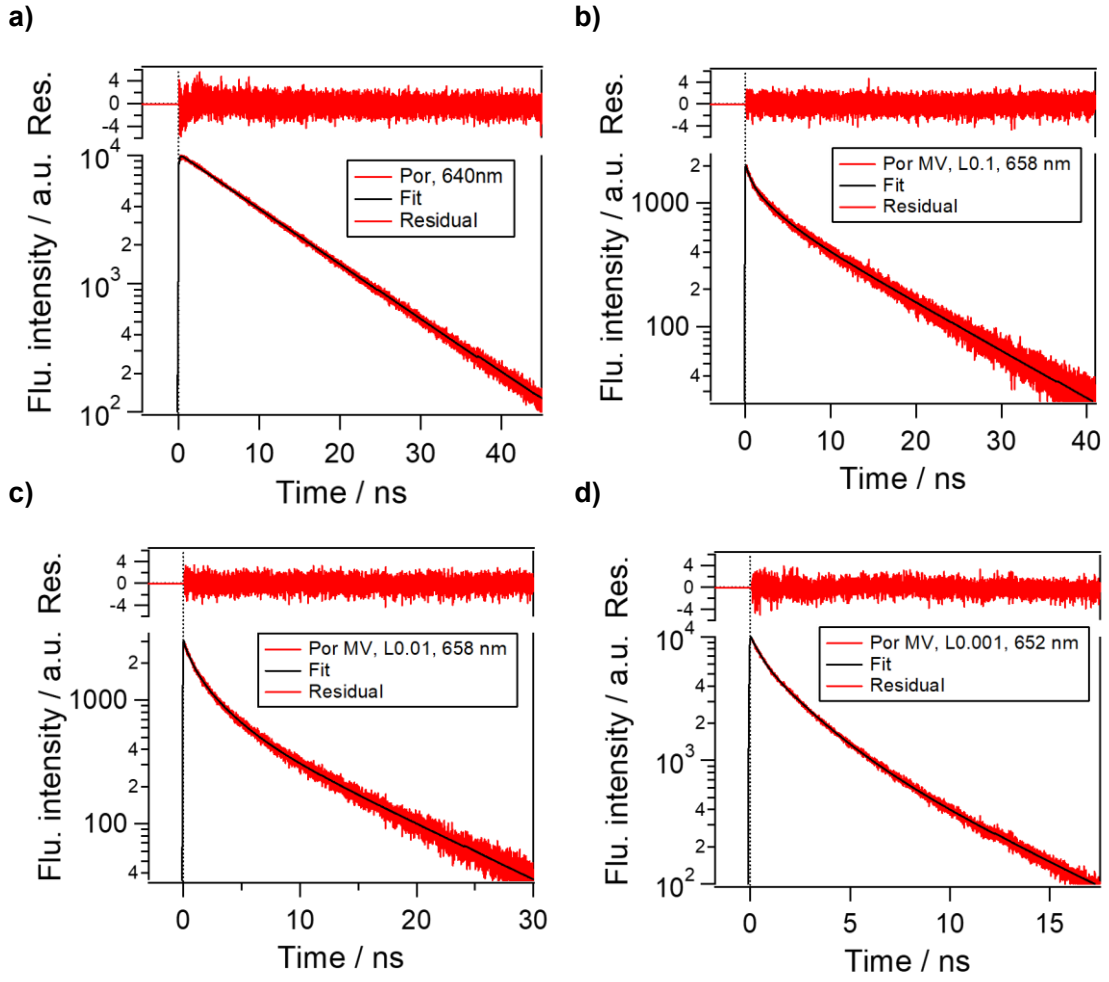

Fig. 3-6. Fluorescence decay profiles of TPPS in the a) absence of P4VPMe and presence of P4VPMe (M_n = 4,300) at varying charge ratios: b) I = 0.10, c) I = 0.01 and d) I = 0.001.

The fluorescence lifetime data were fitted using the equation:

$$I(t) = \sum_{i}^{n} A_i \exp(-t / \tau_i)$$

where $I(t)$ is fluorescence intensity, A_i is corresponding pre-exponential factor in %, t is time and τ_i is fluorescence lifetime. The summarized fluorescence lifetimes are provided in Table 3-1.

Table 3-1. Excited singlet-state lifetimes, τ_i (i = 1–4), of ZnTPPS and TPPS in the absence and presence of P4VPMe. A_i (i = 1–4) are corresponding pre-exponential factors in % and τ_{avg} is averaged lifetime.

Sample	τ_1 / ns	τ_2 / ns	τ_3 / ns	τ_4 / ns	A_1	A_2	A_3	A_4	τ_{avg} / ns
ZnTPPS	1.88				100				1.88
I = 0.10	0.092	0.470	1.62	3.20	69	12	17	2	0.459
I = 0.01	0.289	1.34	2.17		14	44	42		1.54
I = 0.001	0.656	1.50	2.04		18	57	25		1.48
TPPS	10.0				100				10.0
I = 0.10	0.464	2.38	10.8		29	33	38		5.02
I = 0.01	0.472	2.16	9.10		33	46	21		3.06
I = 0.001	0.344	1.80	4.96		37	43	20		1.89

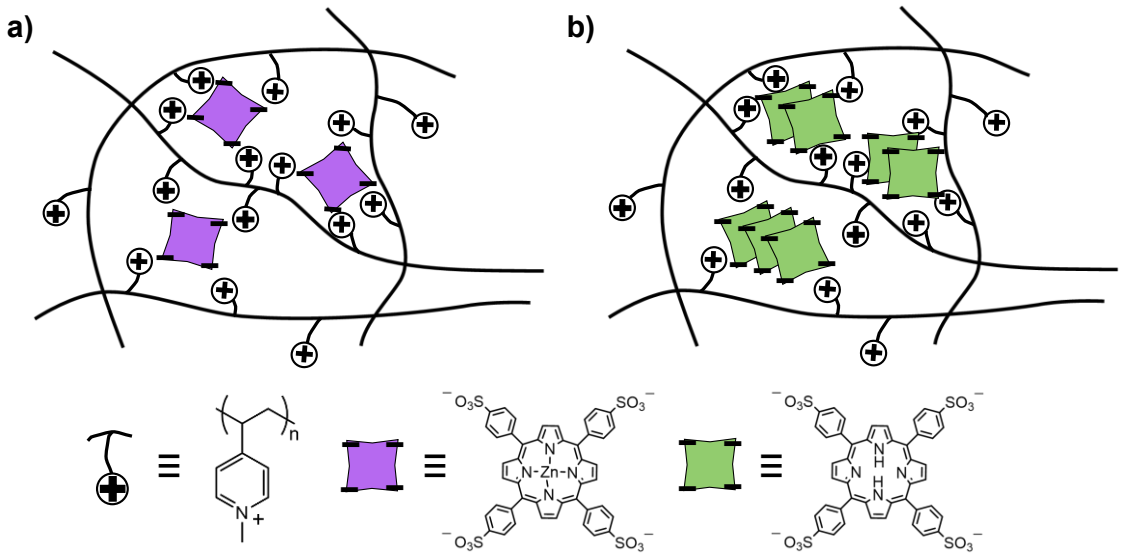

Fig. 3-7. Conceptual figures of a) ZnTPPS exists as individual molecule in P4VPMe matrix and b) TPPS forms aggregates in P4VPMe matrix.

Absorption and excitation spectra were acquired for mixed solutions of ZnTPPS or TPPS (0.6 μM) and P4VPMe (M_n = 7,400) at varying charge ratios (0.10, 0.01 and 0.001) in 0.01 M phosphate buffer (pH 8.0) (Fig. 3-8). Similar spectral changes were observed

when compared with using P4VPMe of M_n = 4,300 indicating no discernible dependency on molecular weight.

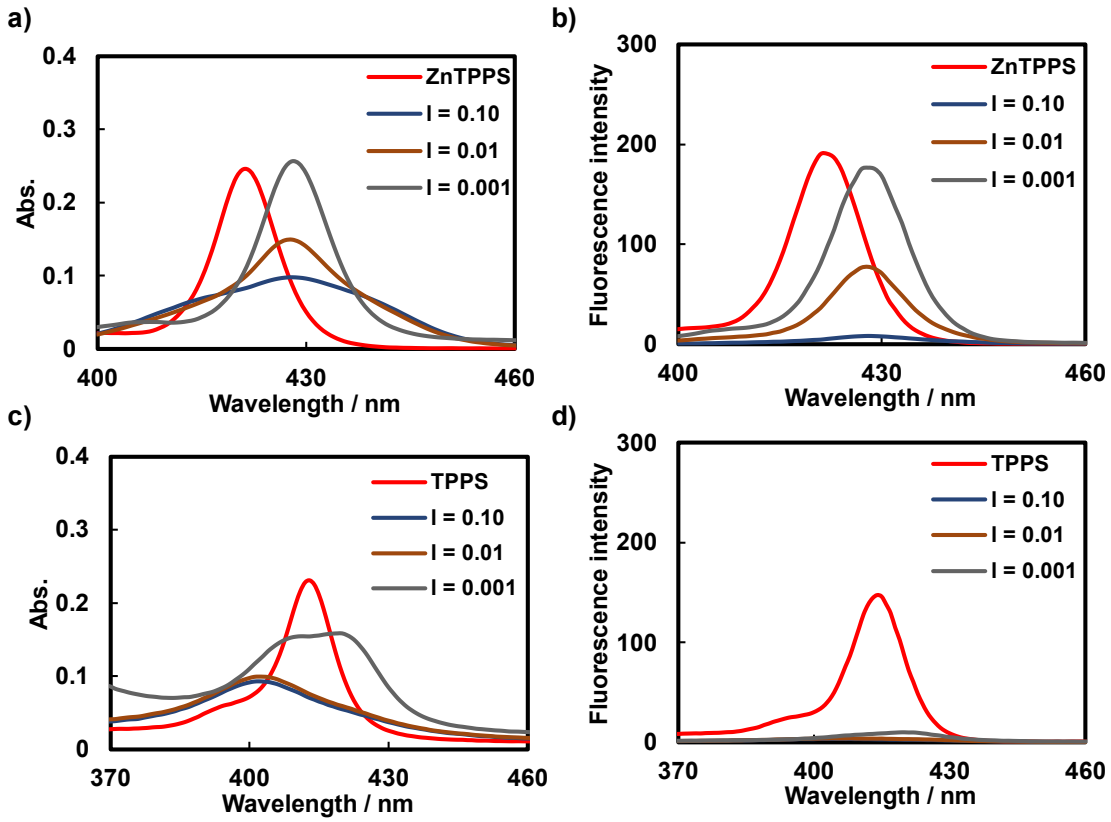

Fig. 3-8. Absorption spectra of a) ZnTPPS and b) TPPS upon the addition of P4VPMe (M_n = 7,400) at varying charge ratios. Excitation spectra of c) ZnTPPS (λ_{em} = 605 nm) and d) TPPS (λ_{em} = 640 nm) upon the addition of P4VPMe (M_n = 7,400) at varying charge ratios.

3-3.2. Charge-transfer complex and photoinduced electron transfer

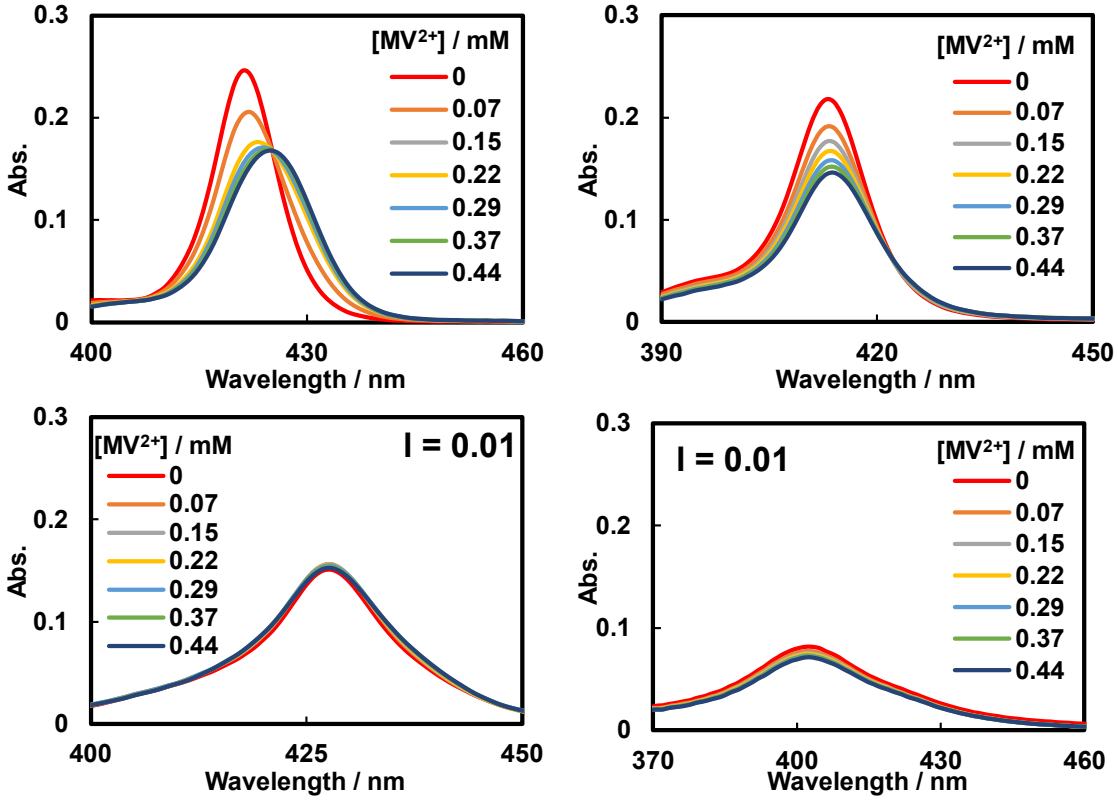

Fig. 3-9. Absorption spectra of a) ZnTPPS and b) TPPS upon the addition of MV^{2+}. Absorption spectra of c) ZnTPPS and d) TPPS upon the addition of MV^{2+} in the presence of P4VPMe (I = 0.01).

ZnTPPS and TPPS are recognized for their ability to form charge-transfer complex with MV^{2+}.[25] When MV^{2+} is added, both ZnTPPS and TPPS exhibit a notable redshift in their Soret bands (Figs. 3-9a and 3-9b), indicating the formation of charge-transfer complex. However, in the presence of P4VPMe (I = 0.01), no significant changes were observed in the Soret bands of either ZnTPPS or TPPS upon the addition of MV^{2+} (Figs. 3-9c and 3-9d). This suggests that P4VPMe hinders the formation of ground-state charge-transfer complex between ZnTPPS or TPPS and MV^{2+}.

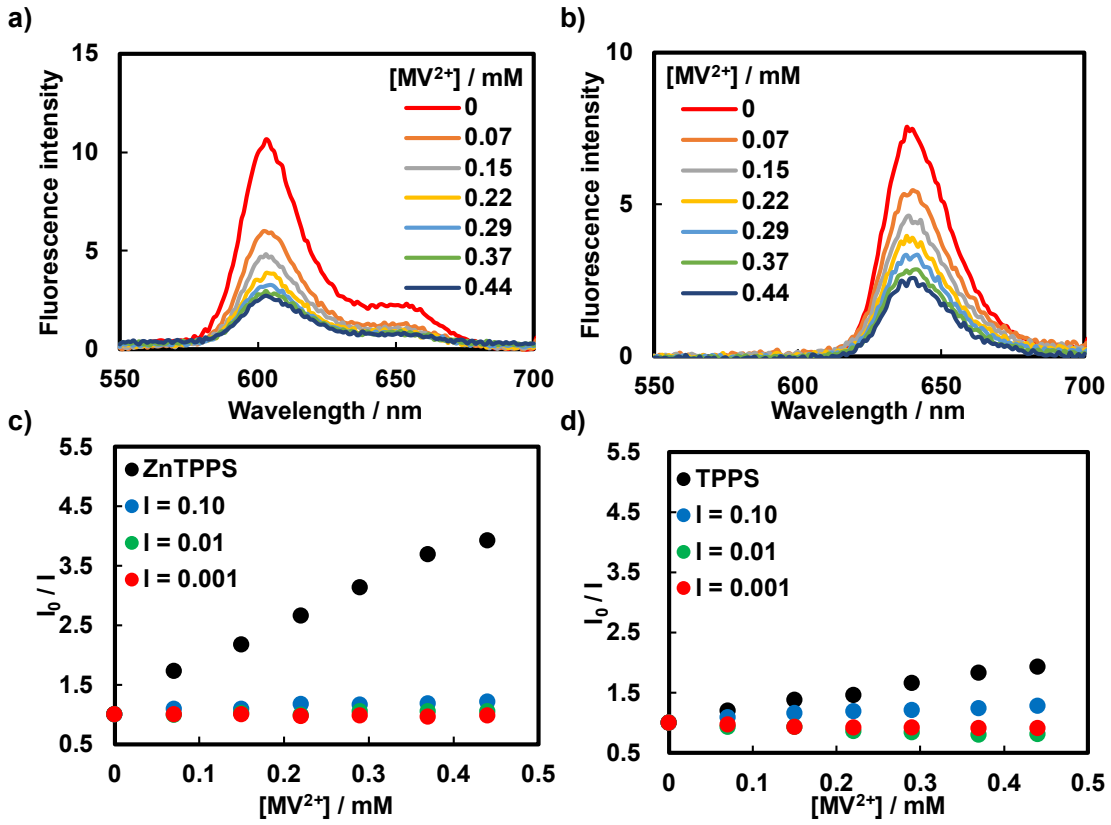

Fig. 3-10. Florescence spectra of a) ZnTPPS and b) TPPS upon the addition of MV^{2+} in the air. Stern-Volmer plots for the quenching of c) ZnTPPS and d) TPPS in the absence and presence of P4VPMe.

The addition of MV^{2+} led to a reduction in the fluorescence intensity of ZnTPPS and TPPS (Figs. 3-10a and 3-10b), a phenomenon commonly referred to as fluorescence quenching. This quenching is attributed to the electron transfer from the excited singlet state of ZnTPPS or TPPS to MV^{2+}. Fluorescence quenching experiments involving ZnTPPS and TPPS in the presence of P4VPMe (M_n = 4,300) in the air were also conducted (Figs. 3-11 and 3-12), and Stern-Volmer plots were constructed based on the fluorescence intensities (Figs. 3-10c, and 3-10d). The slopes of the Stern-Volmer plots,

represented as Stern-Volmer constants (K_{SV}), decreased for both ZnTPPS and TPPS systems following the addition of P4VPMe. This observation suggests that the presence of P4VPMe creates a less favorable environment for photoinduced electron transfer, aligning with the results obtained from absorption spectra which showed a restriction in the formation of ground-state charge-transfer complex. In the case of TPPS, K_{SV} values became negative in the presence of an excess of P4VPMe (I = 0.01 and 0.001). This phenomenon was attributed to the minor partial dissociation of TPPS aggregates within the P4VPMe polymer matrix induced by the addition of MV^{2+}, resulting in a slight increase in fluorescence intensity.

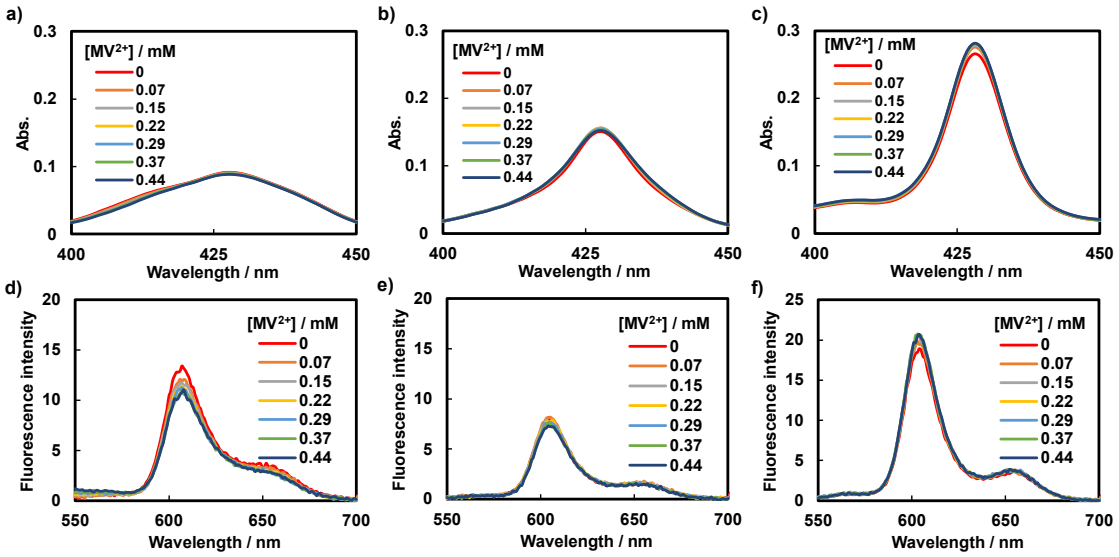

Fig. 3-11. Absorption spectra of ZnTPPS upon incremental addition of MV^{2+} in the presence of P4VPMe (M_n = 4,300) at various charge ratios: a) I = 0.10, b) I = 0.01 and c) I = 0.001. Fluorescence spectra of TPPS upon incremental addition of MV^{2+} in the presence of P4VPMe (M_n = 4,300) at various charge ratios: d) I = 0.10, e) I = 0.01 and f) I = 0.001.

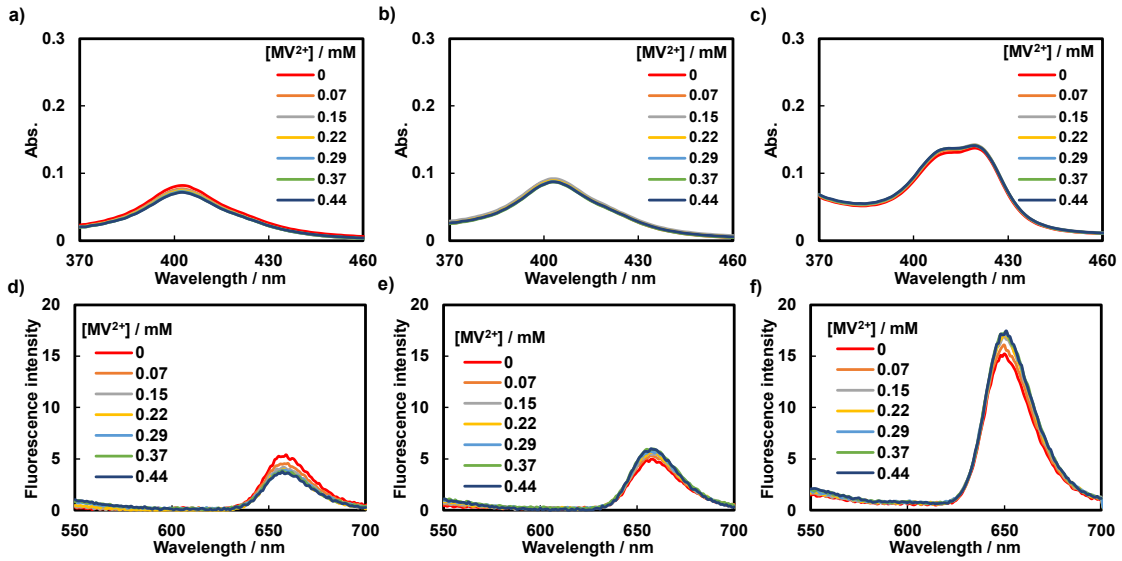

Fig. 3-12. Absorption spectra of TPPS upon incremental addition of MV^{2+} in the presence of P4VPMe (M_n = 4,300) at various charge ratios: a) I = 0.10, b) I = 0.01 and c) I = 0.001. Fluorescence spectra of TPPS upon incremental addition of MV^{2+} in the presence of P4VPMe (M_n = 4,300) at various charge ratios: d) I = 0.10, e) I = 0.01 and f) I = 0.001.

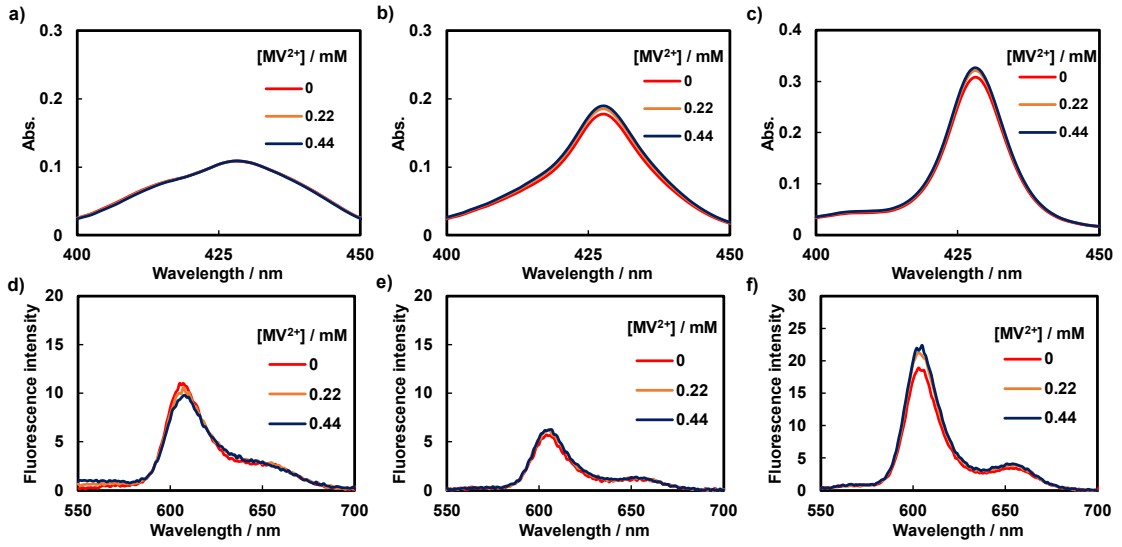

Fig. 3-13. Absorption spectra of ZnTPPS upon incremental addition of MV^{2+} in the presence of P4VPMe (M_n = 7,400) at various charge ratios: a) I = 0.10, b) I = 0.01 and c) I = 0.001. Fluorescence spectra of TPPS upon incremental addition of MV^{2+} in the

presence of P4VPMe (M_n = 7,400) at various charge ratios: d) I = 0.10, e) I = 0.01 and f) I = 0.001.

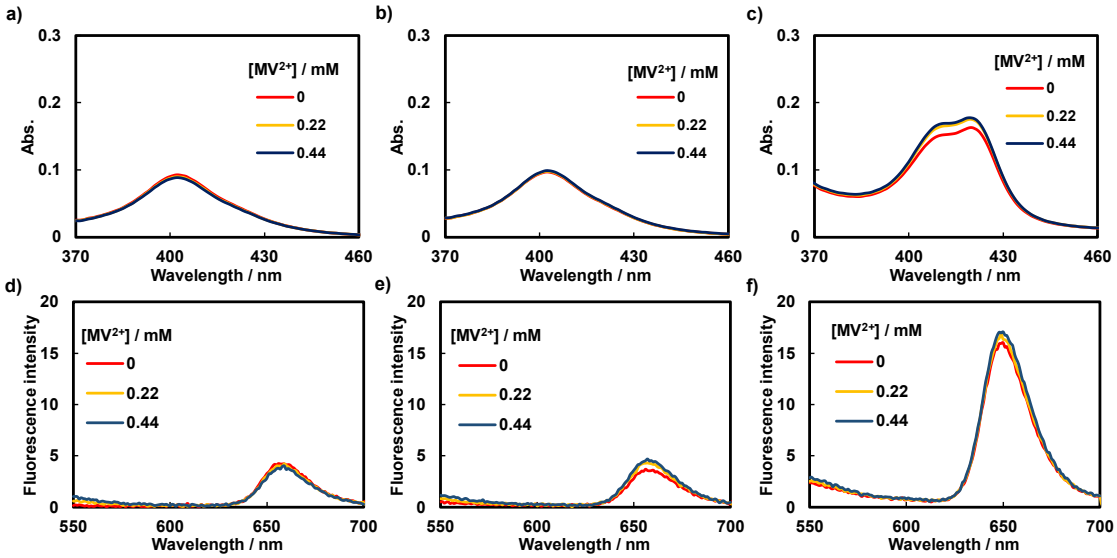

Fig. 3-14. Absorption spectra of TPPS upon incremental addition of MV^{2+} in the presence of P4VPMe (M_n = 7,400) at various charge ratios: a) I = 0.10, b) I = 0.01 and c) I = 0.001. Fluorescence spectra of TPPS upon incremental addition of MV^{2+} in the presence of P4VPMe (M_n = 7,400) at various charge ratios: d) I = 0.10, e) I = 0.01 and f) I = 0.001.

Fluorescence quenching experiments involving ZnTPPS and TPPS in the presence of P4VPMe (M_n = 7,400) in the air were also conducted (Figs. 3-13 and 3-14), and Stern-Volmer plots were constructed based on the fluorescence intensities (Fig. 3-15). Notably, the quenching behavior of ZnTPPS or TPPS in the presence of P4VPMe with different molecular weights remained relatively consistent, suggesting an absence of molecular weight dependency when M_n = 4,300 or 7,400.

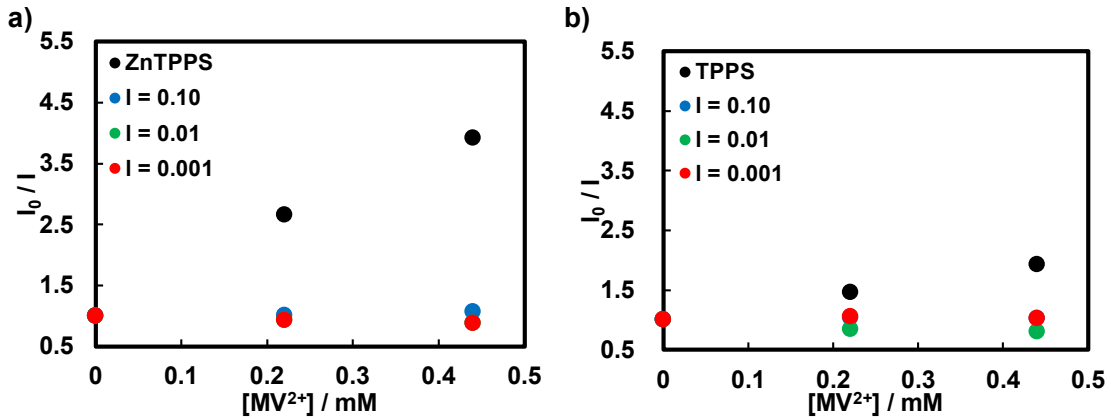

Fig. 3-15. Stern-Volmer plots for the quenching of a) ZnTPPS and b) TPPS by MV^{2+} in the absence and presence of P4VPMe (M_n = 7,400).

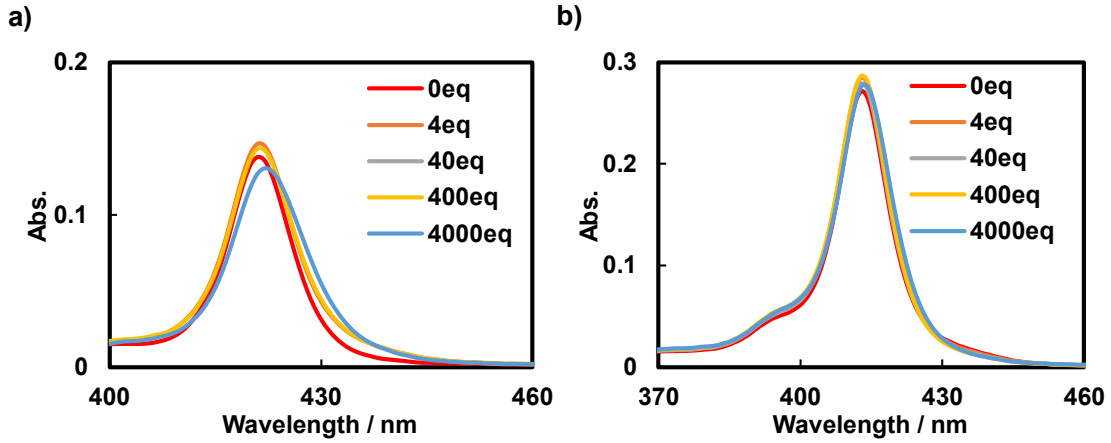

Fig. 3-16. Absorption spectra of a) ZnTPPS and b) TPPS upon the addition of DMP. The amounts of added DMP are indicated in the figures.

Absorption spectra were obtained for mixed solutions of ZnTPPS or TPPS (0.6 μM) and 1,4-dimethylpyridinium (DMP) at different mixing ratios in a 0.01 M phosphate buffer (pH 8.0) (Fig. 3-16). Notably, no systematic spectral changes were observed, indicating that the interaction between DMP and ZnTPPS or TPPS is weak and lacks influence on their aggregate states, a contrast to the impact P4VPMe exerts.

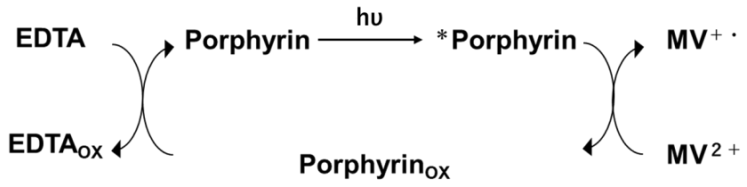

Scheme 3-2. Generation of $MV^{+\bullet}$ from MV^{2+} via electron transfer from photoexcited porphyrin with EDTA as a sacrificial agent.

Ethylenediamine-*N*,*N*,*N*′,*N*′-tetraacetic acid tetrasodium salt (EDTA) was employed as a sacrificial agent to enable the reduction of oxidized ZnTPPS or TPPS after the photoinduced electron transfer process (Scheme 3-2). This allowed us to conduct continuous photoinduced electron transfer experiments. Deoxygenated solutions containing ZnTPPS or TPPS, P4VPMe (M_n = 4,300, I = 0.01), MV^{2+}, and EDTA were exposed to light ($\lambda > 400$ nm) at an intensity of ca. 3 mW cm^{-2} for a duration of 30 min. The quantities of generated methylviologen cation radical ($MV^{+\bullet}$) were determined by monitoring the change in absorbance at 605 nm, a characteristic absorption wavelength of $MV^{+\bullet}$, in conjunction with its molar absorption coefficient (Fig. 3-17).[26]

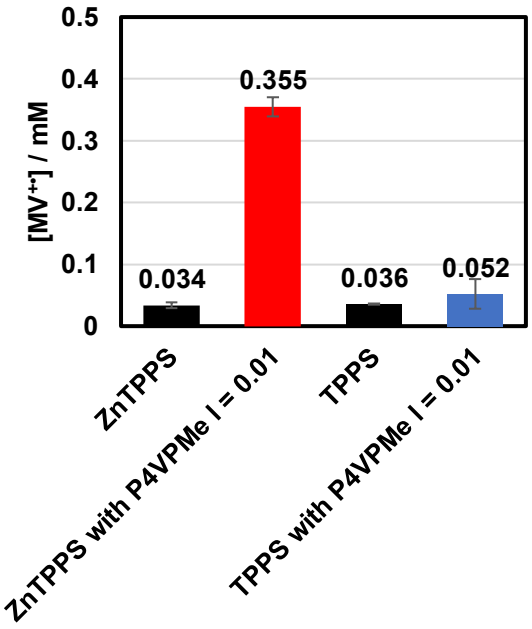

Fig. 3-17. Generated $MV^{+\bullet}$ in ZnTPPS and TPPS systems, in the absence and presence of P4VPMe.

Within the P4VPMe polymer matrix, ZnTPPS exhibited over a tenfold increase in the generation of $MV^{+\bullet}$ compared to ZnTPPS alone, without P4VPMe. In contrast, the catalytic activity for the photoinduced oxidation of MV^{2+} by TPPS remained relatively unchanged in the presence or absence of P4VPMe. This difference can be attributed to the distinct aggregate states of ZnTPPS and TPPS within P4VPMe. The aggregation states within the polymer matrix play a crucial role in this difference. When aggregated, absorbed photon energy tends to dissipate as thermal energy rather than participating in photoinduced electron transfer.

Additional experiments were conducted to compare the outcomes between P4VPMe variants with distinct M_n's of 4,300 and 7,400 at different charge ratios (I = 4.00, 2.00, 0.10, 0.01 and 0.001) (Figs. 3-18, 3-19, 3-20, and 3-21) beyond the previously discussed

experiment using P4VPMe with M_n = 4,300 at a charge ratio of 0.01. The concentrations of the resulting $MV^{+\bullet}$ were collated and presented in Fig. 3-23.

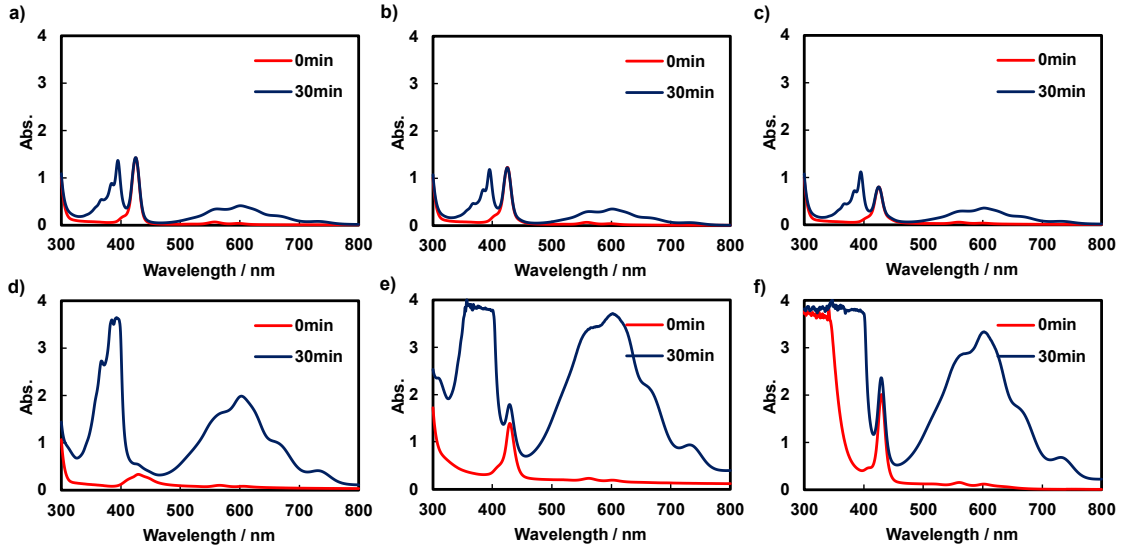

Fig. 3-18. Absorption spectra of mixing solutions of ZnTPPS, MV^{2+}, EDTA-4Na before and after 30 min irradiation in the a) absence of P4VPMe and b)-f) presence of P4VPMe (M_n = 4,300) at various charge ratios: b) I = 4.00, c) I = 2.00, d) I = 0.10, e) I = 0.01 and f) I = 0.001.

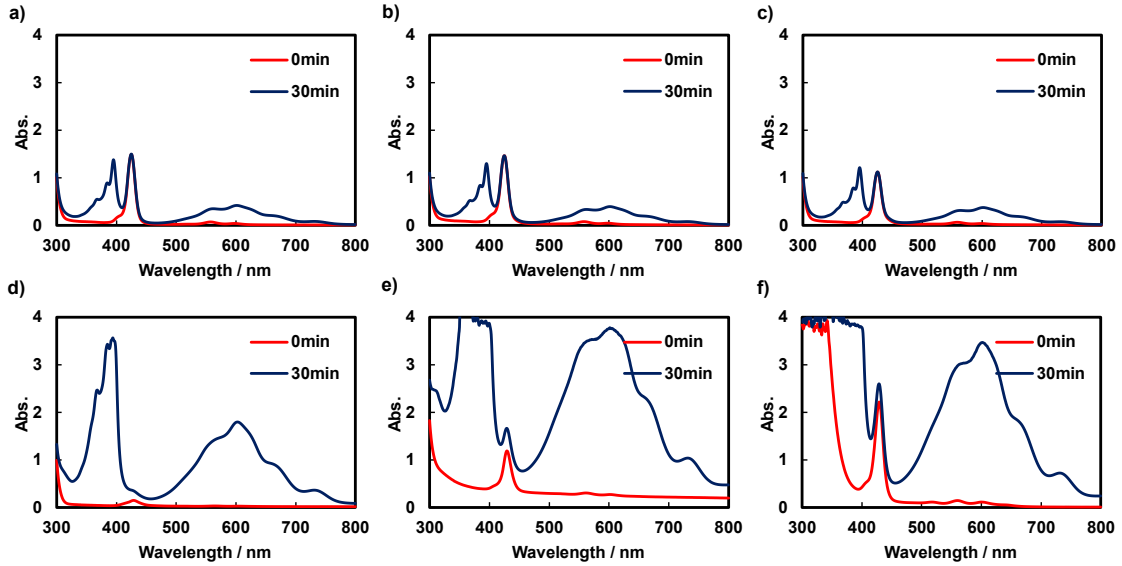

Fig. 3-19. Absorption spectra of mixing solutions of ZnTPPS, MV^{2+}, EDTA-4Na before and after 30 min irradiation in the a) absence of P4VPMe and b)-f) presence of P4VPMe (M_n = 7,400) at various charge ratios: b) I = 4.00, c) I = 2.00, d) I = 0.10, e) I = 0.01 and f) I = 0.001.

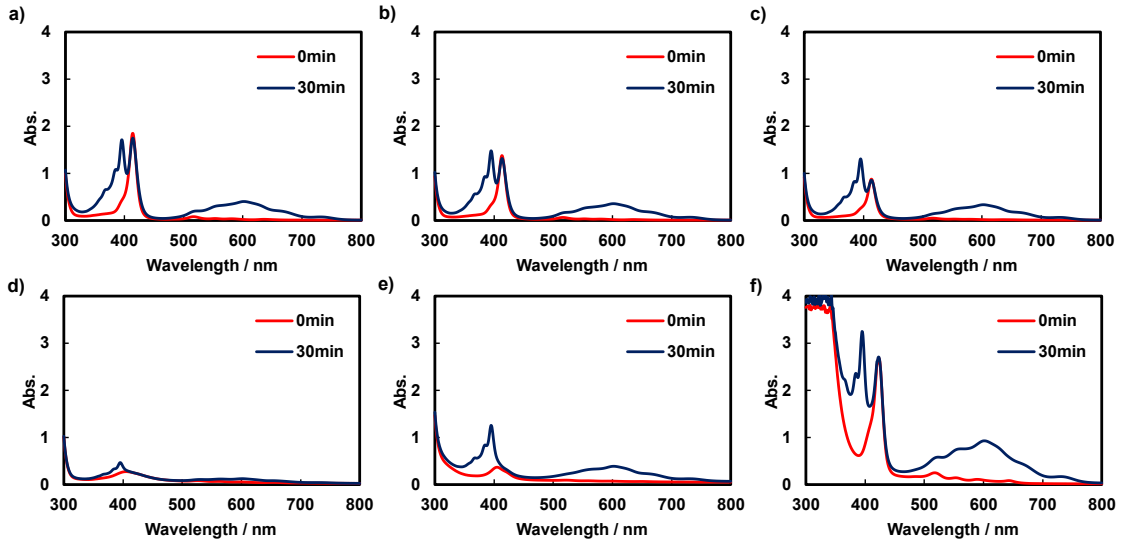

Fig. 3-20. Absorption spectra of mixing solutions of TPPS, MV^{2+}, EDTA-4Na before and after 30 min irradiation in the a) absence of P4VPMe and b)-f) presence of P4VPMe (M_n = 4,300) at various charge ratios: b) I = 4.00, c) I = 2.00, d) I = 0.10, e) I = 0.01 and f) I

= 0.001.

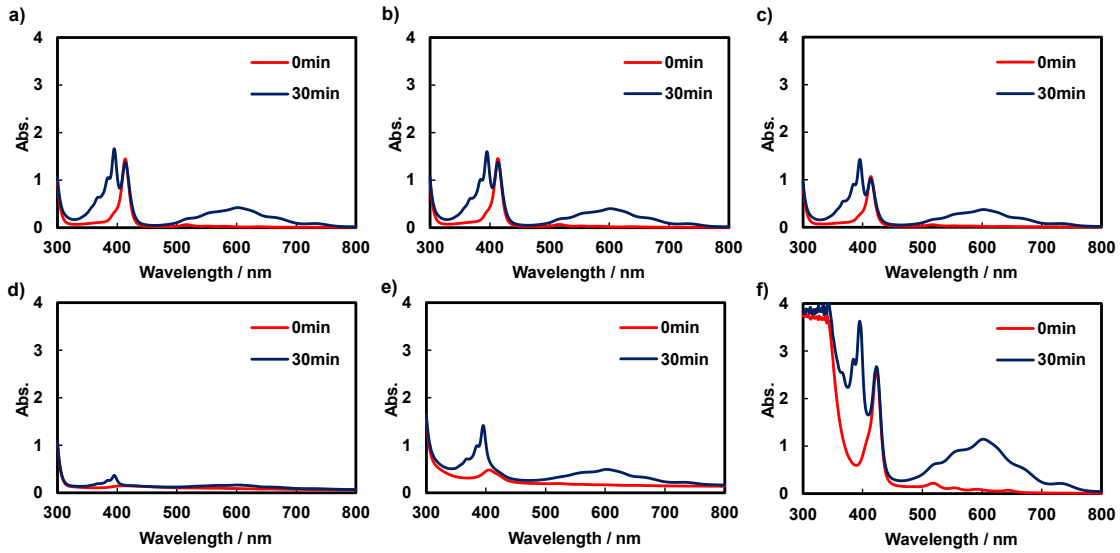

Fig. 3-21. Absorption spectra of mixing solutions of TPPS, MV^{2+}, EDTA-4Na before and after 30 min irradiation in the a) absence of P4VPMe and b)-f) presence of P4VPMe (M_n = 7,400) at various charge ratios: b) I = 4.00, c) I = 2.00, d) I = 0.10, e) I = 0.01 and f) I = 0.001.

$MV^{+\bullet}$ generation experiments were conducted for ZnTPPS and TPPS in the presence of DMP (Fig. 22), and the resulting concentrations of generated $MV^{+\bullet}$ were presented in Fig. 3-23.

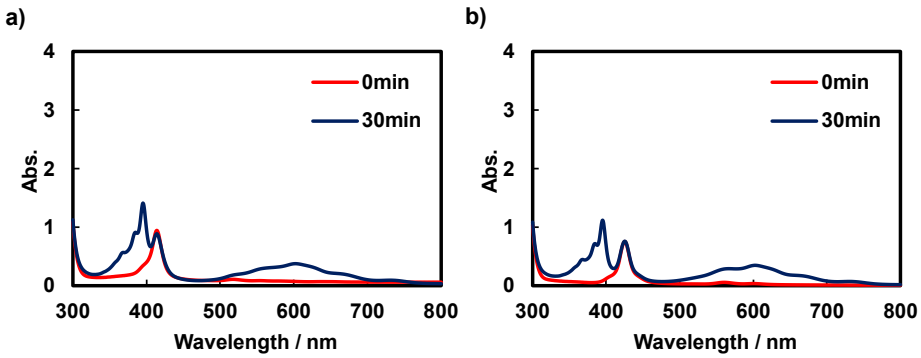

Fig. 3-22. Absorption spectra of a) mixing solutions of ZnTPPS, MV^{2+}, EDTA-4Na and DMP, and b) mixing solutions of TPPS, MV^{2+}, EDTA-4Na and DMP before and after 30 min irradiation.

For the ZnTPPS systems, the quantity of generated $MV^{+\bullet}$ generally increased with the P4VPMe concentration, except for a decrease observed at a charge ratio of 0.001. This decline was attributed to the electrostatic repulsion between MV^{2+} and an excessive amount of P4VPMe, making it less favorable for MV^{2+} to approach ZnTPPS. In the case of TPPS systems, the quantity of generated $MV^{+\bullet}$ remained relatively consistent, with the lowest and highest amounts observed at charge ratios of 0.10 and 0.001, respectively. These ratios align with TPPS exhibiting its most aggregated and most disassociated states during the experiments. DMP exhibited no or only a few effect on the generation of $MV^{+\bullet}$, underscoring the crucial role of P4VPMe in modulating the aggregate state of porphyrins and their photoinduced electron transfer to MV^{2+}.

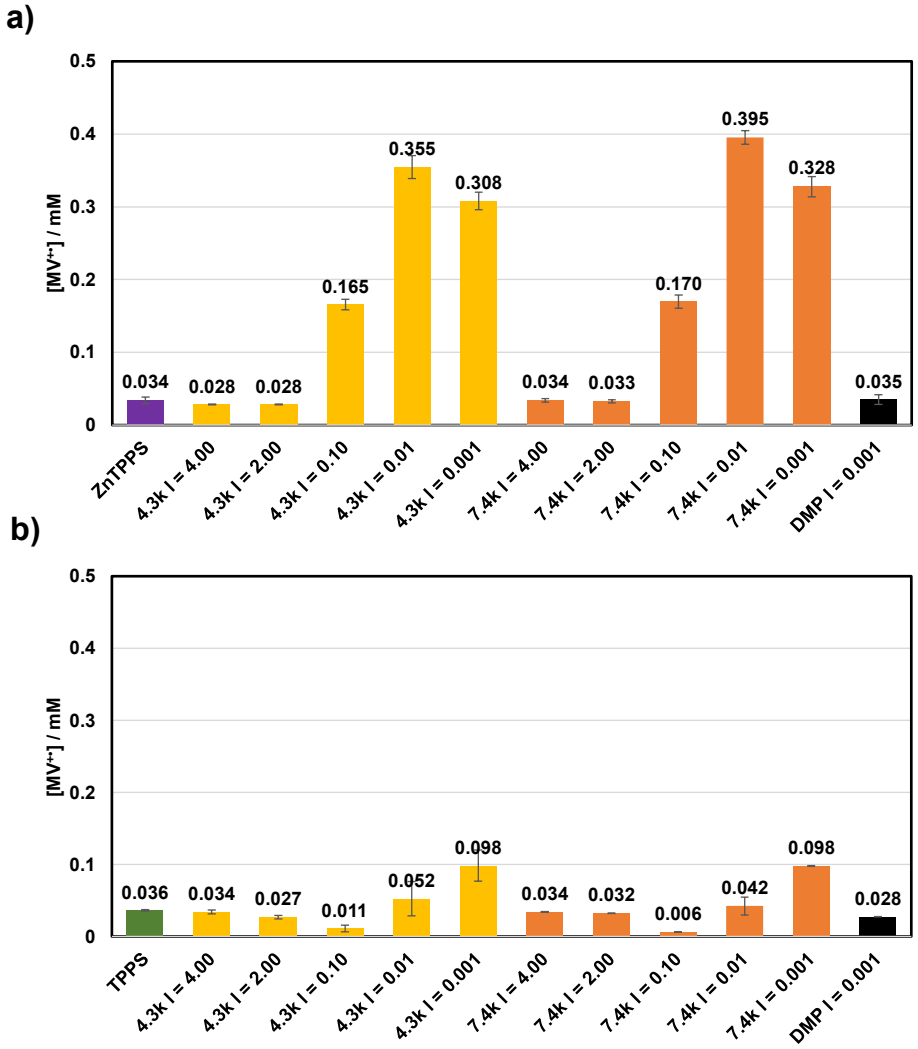

Fig. 3-23. Concentration of generated $MV^{+\bullet}$ after 30 min irradiation in a) ZnTPPS systems and b) TPPS systems.

Although ZnTPPS exists as individual molecule within the P4VPMe matrix ($I = 0.01$), favoring the photoinduced electron transfer process, it predominantly occurs from the singlet excited state. However, the photoinduced electron transfer process from the singlet state results in a minimal generation of $MV^{+\bullet}$, as evidenced by the near-zero K_{SV}, indicating only a limited electron transfer from the singlet state of ZnTPPS to MV^{2+}. The primary photoinduced electron transfer pathway in this system may involve the triplet

state under the deoxygenated conditions. To investigate this process, transient absorption spectra were recorded.

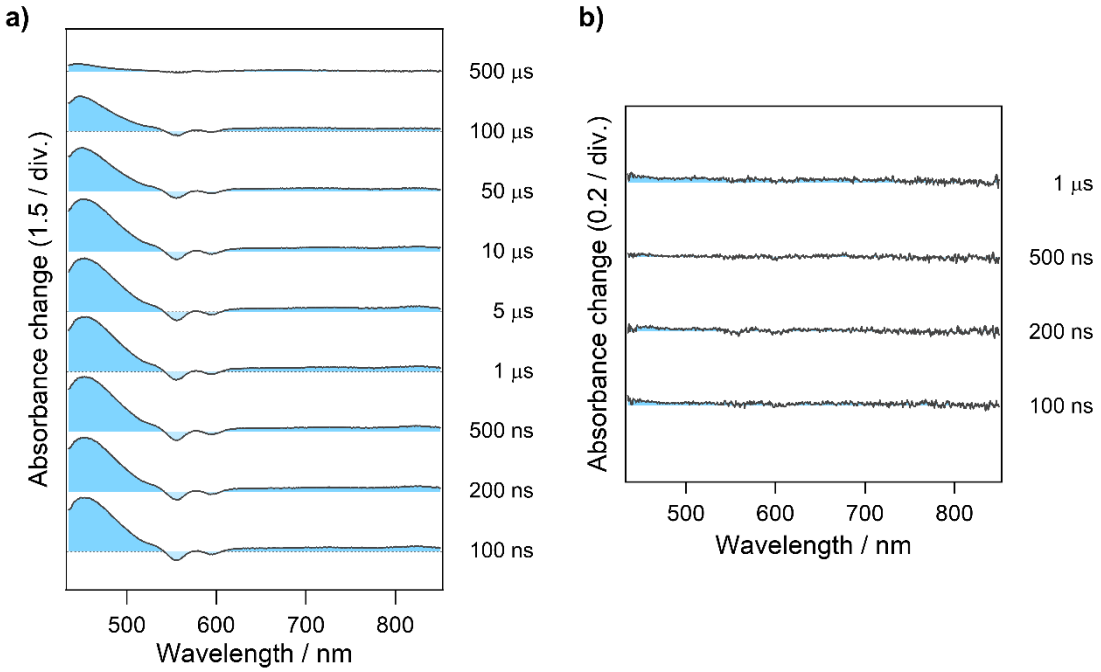

Fig. 3-24. Transient absorption spectra of a) ZnTPPS and b) ZnTPPS with MV^{2+} in the nanosecond and microsecond time regions. The sample solution was deoxygenated with nitrogen bubbling before the measurements.

For ZnTPPS, an absorption band originating from the triplet state of the ZnTPPS was observed approximately 100 ns after photoexcitation, appearing in the region below 540 nm (Fig. 3-24a). This characteristic band persisted for several hundreds of microseconds before showing a partial decay at ca. 500 µs, corresponding to the intrinsic triplet state lifetime of ZnTPPS.[27] However, when MV^{2+} was added to this ZnTPPS system, no transient absorption signals were detected (Fig. 3-24b). In this scenario, even if a charge-transfer state is formed after photoexcitation, it rapidly recombines to the ground state

within the temporal resolution of the current measurement. Consequently, no distinct signals were observed in the transient absorption spectrum.

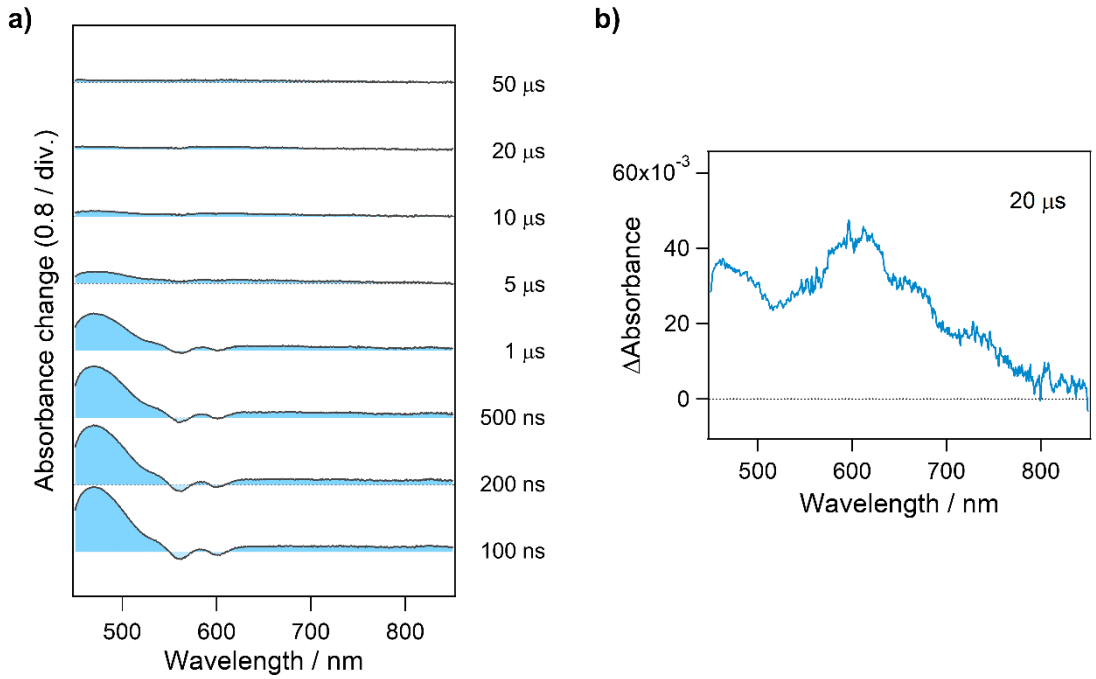

Fig. 3-25. a) Transient absorption spectra of mixing solution of ZnTPPS, MV^{2+}, and P4VPMe in the nanosecond and microsecond time regions. b) Enlarged spectrum recorded at 20 μs. The sample solution was deoxygenated with nitrogen bubbling before the measurements.

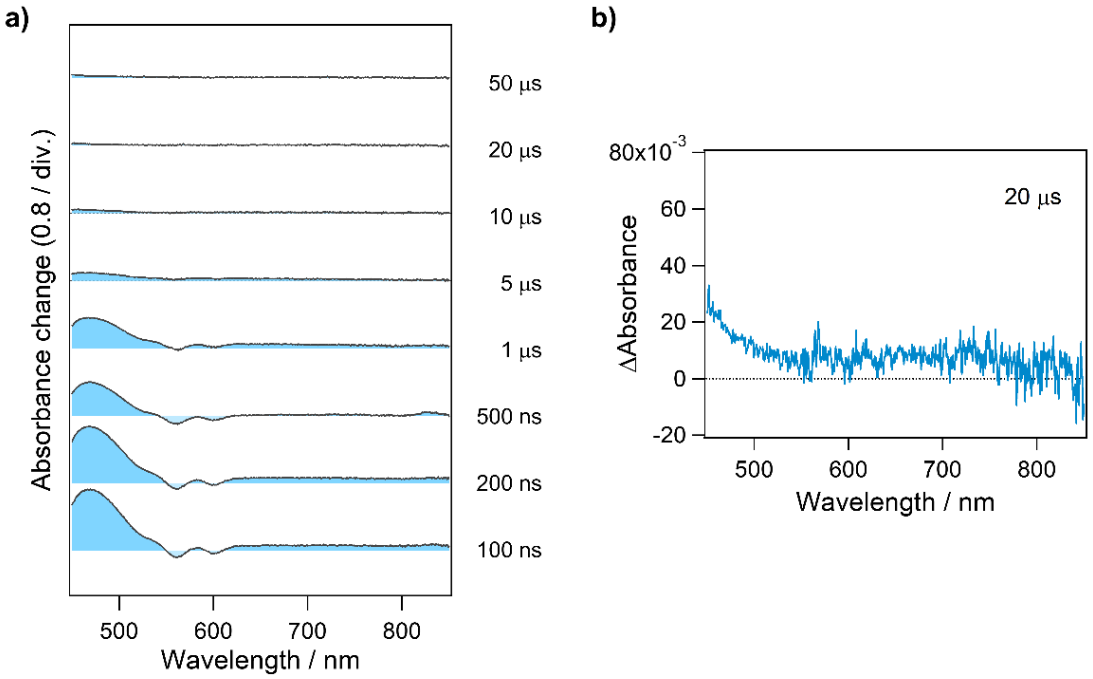

Fig. 3-26 a) Transient absorption spectra of mixing solution of ZnTPP, MV^{2+}, and P4VPMe in the nanosecond and microsecond time regions. b) Enlarged spectrum recorded at 20 µs. The sample solution was air-saturated.

In the ZnTPPS, P4VPMe, and MV^{2+} system, the triplet absorption band of porphyrin was initially observed upon excitation and decays over a time scale of a few microseconds (Fig. 3-25a). Additionally, upon further enlargement of the transient absorption spectrum after this time, the appearance of the $MV^{+\bullet}$ absorption band, believed to be generated by electron transfer, was detected (Fig. 3-25b). It should be noted that this $MV^{+\bullet}$ absorption band was not observed under the air-saturated conditions where molecular oxygen effectively quenches the triplet state (Fig. 3-26b). This observation strongly suggests that electron transfer from the triplet state of ZnTPPS to MV^{2+} indeed occurs.

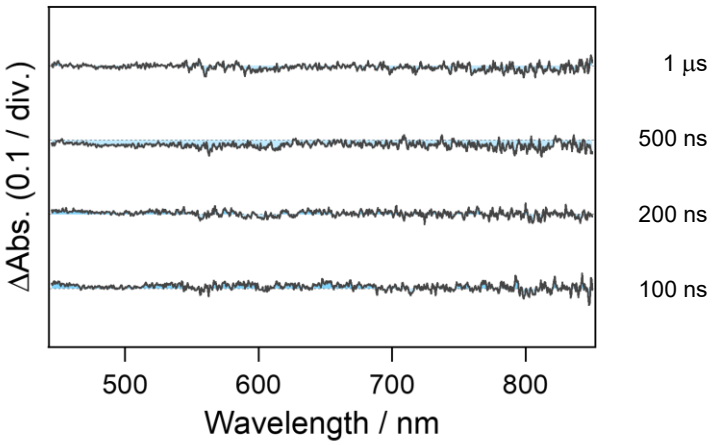

Fig. 3-27. Transient absorption spectra of mixing solution of ZnTPPS, MV^{2+}, and PAA in the nanosecond and microsecond time regions.

Transient absorption spectra were obtained for a mixing solution of ZnTPPS (0.12 mM), MV^{2+} (0.02 M), and polyacrylic acid (PAA, 48.0 mM, I = 0.01) (Fig. 3-27). However, no transient absorption was detected, indicating that PAA lacks the capacity to impede the formation of charge-transfer complexes between ZnTPPS and MV^{2+}, a phenomenon effectively demonstrated by P4VPMe.

3-4. Conclusion

In summary, our study has uncovered intricate electron transfer dynamics within the porphyrin, polymer, and MV^{2+} system. The presence of P4VPMe amplified $MV^{+\bullet}$ generation from ZnTPPS, underscoring the pivotal role of the polymer matrix. This effect is linked to the distinct aggregate states of ZnTPPS and TPPS within P4VPMe. Transient absorption studies revealed the dynamic electron transfer from the triplet state of ZnTPPS to MV^{2+}. Our research thus yielded valuable insights into electron transfer dynamics and

their interplay with polymer matrices, potentially impacting photochemical and photophysical applications.

References

1. Balzani, V.; Credi, A.; Venturi, M. *ChemSusChem.* **2008**, *1*, 26–58.
2. Breuer, M.; Rosso, K.; Blumberger, J. *Proc. Natl. Acad. Sci. U.S.A.* **2014**, *111*, 611–616.
3. Rajak, S.; Vu, N.; Kaur, P.; Duong, A.; Nguyen-Tri, P. *Coord. Chem. Rev.* **2022**, *456*, 214375.
4. Yoshimura, N.; Yoshida, M.; Kobayashi, A. *J. Am. Chem. Soc.* **2023**, *145*, 6035–6038.
5. Wasielewski, M. *Acc. Chem. Res.* **2009**, *42*, 1910–1921.
6. Fukuzumi, S.; Fujioka, N.; Kotani, H.; Ohkubo, K.; Lee, Y.; Nam, W. *J. Am. Chem. Soc.* **2009**, *131*, 17127–17134.
7. Cao, Y.; Takasaki, T.; Yamashita, S.; Mizutani, Y.; Harada, A.; Yamaguchi, H. *Polymers* **2022**, *14*, 1191.
8. Frühbeisser, S.; Gröhn, F. *J. Am. Chem. Soc.* **2012**, *134*, 14267–14270.
9. Krieger, A.; Werner, J.; Mariani, G.; Gröhn, F. *Macromolecules* **2017**, *50*, 3464–3475.
10. Sadamoto, R.; Tomioka, N.; Aida, T. *J. Am. Chem. Soc.* **1996**, *118*, 3978–3979.
11. Wang, R.; Qu, R.; Jing, C.; Zhai, Y.; An, Y.; Shi, L. *RSC Adv.* **2017**, *7*, 10100–10107.
12. Wang, X.; Zhao, L.; Ma, R.; An, Y.; Shi, L. *Chem. Commun*. **2010**, *46*, 6560–6562.
13. Higashino, T.; Kawamoto, K.; Sugiura, K.; Fujimori, Y.; Tsuji, Y.; Kurotobi, K.; Ito, S.; Imahori, H. *ACS Appl. Mater. Interfaces* **2016**, *8*, 15379–15390.
14. Zhang, A.; Li, C.; Yang, F.; Zhang, J.; Wang, Z.; Wei, Z.; Li, W. *Angew. Chem. Int. Ed.* **2017**, *56*, 2694–2698.
15. Zhou, D.; Wang, J.; Xu, Z.; Xu, H.; Quan, J.; Deng, J.; Li, Y.; Tong, Y.; Hu, B.; Chen, L. *Nano Energy* **2022**, *103*, 107802.
16. Fu, C.; Sun, X.; Zhang, G.; Shi, P.; Cui, P. *Inorg. Chem.* **2021**, *60*, 1117–1124.

17. Wirojsaengthong, S.; Aryuwananon, D.; Aeungmaitrepirom, W.; Pulpoka, B.; Tuntulani, T. *Talanta* **2021**, *231*, 122371.
18. Frolova, L.; Furmansky, Y.; Shestakov, A.; Emelianov, N.; Liddell, P.; Gust, D.; Visoly-Fisher, I.; Troshin, P. *ACS Appl. Mater. Interfaces* **2022**, *14*, 15461–15467.
19. Xiang, D.; Wang, X.; Jia, C.; Lee, T.; Guo, X. *Chem. Rev.* **2016**, *116*, 4318–4440
20. Flamigni, L.; Talarico, A.; Ventura, B.; Rein, R.; Solladié, N. *Chem. Eur. J.* **2006**, *12*, 701–712.
21. Nagasawa, Y.; Itoh, T.; Yasuda, M.; Ishibashi, Y.; Ito, S.; Miyasaka, H. *J. Phys. Chem. B* **2008**, *112*, 15758–15765.
22. Sotome, H.; Kitagawa, D.; Nakahama, T.; Ito, S.; Kobatake, S.; Irie, M.; Miyasaka, H. *Phys. Chem. Chem. Phys.* **2019**, *21*, 8623–8632.
23. Maiti, N.; Mazumdar, S.; Periasamy, N. *J. Phys. Chem. B* **1998**, *102*, 1528–1538.
24. Ruthard, C.; Maskos, M.; Kolb, U.; Gröhn, F. *J. Phys. Chem. B* **2011**, *115*, 5716–5729.
25. Logunov, S.; Rodgers, M. *J. Photochem. Photobiol. A Chem.* **1997**, *105*, 55–63.
26. Watanabe, T.; Honda, K. *J. Phys. Chem.* **1982**, *86*, 2617–2619
27. Rougee, M.; Ebbesen, T.; Ghetti, F.; Bensasson, R. *J. Phys. Chem.* **1982**, *86*, 4404–4412.

Chapter 4

Summary and Conclusions

In this thesis the author focuses on refining and comprehending the mechanism in supramolecular electron transfer systems within polymer matrices.

Chapter 2 treats with the construction of a photoinduced electron transfer system through the complexation of PVP with TPPS or ZnTPPS. This novel approach controlled the interactions between ground-state porphyrins and MV^{2+}, regulating the photoinduced electron transfer from porphyrins to MV^{2+}. Notably, the introduction of PVP significantly amplified the production of the photoinduced electron transfer product $MV^{+\bullet}$.

Chapter 3 treats with an artificial photoinduced electron transfer system within a P4VPMe polymer matrix. This system features TPPS and ZnTPPS as electron donors and MV^{2+} as the electron acceptor. The presence of P4VPMe amplified $MV^{+\bullet}$ generation from ZnTPPS, underscoring the pivotal role of the polymer matrix. This effect is linked to the distinct aggregate states of ZnTPPS and TPPS within P4VPMe. Transient absorption studies revealed the dynamic electron transfer from the triplet state of ZnTPPS to MV^{2+}.

In conclusion, this thesis has found and investigated several supramolecular electron transfer systems within polymer matrices. Chapters 2 and 3 have highlighted the influential role of polymer matrices (PVP and P4VPMe) in regulating and enhancing photoinduced electron transfer systems. These insights underscore the critical role of

polymer environments in modulating and optimizing electron transfer processes, laying a foundation for future advancements in this field.

List of Publications

1. Cao, Y.; Takasaki, T.; Yamashita, S.; Mizutani, Y.; Harada, A.; Yamaguchi, H. Control of Photoinduced Electron Transfer Using Complex Formation of Water-Soluble Porphyrin and Polyvinylpyrrolidone. *Polymers* **2022**, *14*, 1191. (Chapter 2)

2. Cao, Y.; Sotome, H.; Kobayashi, Y.; Ito, S.; Yamaguchi, H. Controlled Photoinduced Electron Transfer via Triplet in Polymer Matrix Using Electrostatic Interactions. *Submitted*. (Chapter 3)